Energy 300 (2024) 131580

Contents lists available at ScienceDirect

Energy

journal homepage: www.elsevier.com/locate/energy

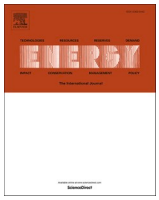

Review

CO_2 gas hydrate for carbon capture and storage applications – Part 2

Morteza Aminnaji [a,b,c,*], M Fahed Qureshi [d], Hossein Dashti [e,f], Alfred Hase [b], Abdolali Mosalanejad [g], Amir Jahanbakhsh [h,i,**], Masoud Babaei [c], Amirpiran Amiri [j], Mercedes Maroto-Valer [h,i]

[a] Institute of GeoEnergy Engineering, Heriot-Watt University, Edinburgh, EH14 4AS, UK
[b] ChampionX, Bundrant Technology Centre, Peterseat Drive, Aberdeen, AB12 3HT, UK
[c] Department of Chemical Engineering and Analytical Science, University of Manchester, Manchester, M13 9PL, UK
[d] Department of Chemical and Biomolecular Engineering, National University of Singapore, Singapore, 117580, Singapore
[e] APA Group, 80 Ann St, Brisbane, QLD, 4000, Australia
[f] School of Chemical Engineering, The University of Queensland, Brisbane, QLD, 4072, Australia
[g] Department of Petroleum Engineering, School of Chemical and Petroleum Engineering, Shiraz University, Shiraz, Iran
[h] The Research Centre for Carbon Solutions (RCCS), School of Engineering and Physical Sciences, Heriot-Watt University, Edinburgh, UK
[i] Industrial Decarbonisation Research and Innovation Centre (IDRIC), Heriot-Watt University, Edinburgh, UK
[j] Energy and Bioproducts Research Institute (EBRI), College of Engineering and Applied Science, Aston University, UK

ARTICLE INFO

Handling Editor: Ruzhu Wang

ABSTRACT

CO_2 hydrate offers some substantial applications for Carbon Capture and Storage (CCS). While CO_2 hydrate chemistry and CO_2 capture are reviewed in part 1 of this review, CO_2 transportation and storage are discussed in this part. Basically, CO_2 transportation is required between CO_2 capture plants and CO_2 sequestration sites. It is imperative to acknowledge that most strategies for achieving deep decarbonization are linked to the expansion of the current transport infrastructure. When dealing with substantial distances between CO_2 capture plants and CO_2 sequestration sites, the expenses associated with CO_2 transportation can surpass the capture process itself. Therefore, despite the benefits of CO_2 hydrates in CCS, challenges, such as flow assurance issues, may arise. For example, CO_2 hydrate formation can lead to pipeline blockages, emphasizing the need for CO_2 gas hydrate flow assurance study as discussed in this part.

Additionally, site selection for CO_2 storage requires careful consideration. Geological storage, whether in hydrate form or through the injection of CO_2 or high-CO_2 content mixtures, offers potential advantages, such as long-term storage and self-sealing capabilities. However, there are some challenges like CO_2 hydrate processes in porous media, injectivity, flow behaviour in hydrate reservoirs, mechanical behaviour, etc., which are discussed in this review.

1. Introduction

Part 1 of this review provides a fundamental understanding of advancements in CO_2 gas hydrate chemistry and technologies, which hold significant potential for CO_2 capture applications. The increasing global attention towards Carbon Capture and Storage (CCS) has led to rapid growth in research, advances, and developments in sustainable hydrate-based technologies.

The focus in this part is on CO_2 hydrate flow assurance, a key research area of hydrate aiming to prevent or minimize the risk of hydrate blockage in pipelines. There are still challenges in reducing the risk of CO_2 hydrate formation during transportation. CO_2, typically captured from major point sources like power generation plants utilizing fossil fuels, is transported through pipelines or ships for secure storage. Consequently, this part provides CO_2 hydrate flow assurance challenges, including dehydration requirements for CO_2 hydrate inhibition, CO_2 hydrate inhibitors, and CO_2 hydrate slurry and blockage. Additionally, CO_2 hydrates present an opportunity for permanent CO_2 storage in geological formations, for example by CH_4–CO_2 replacement in permafrost gas hydrate reservoirs. Therefore, this part also explores the

* Corresponding author. Institute of GeoEnergy Engineering, Heriot-Watt University, Edinburgh, EH14 4AS, UK.
** Corresponding author. The Research Centre for Carbon Solutions (RCCS), School of Engineering and Physical Sciences, Heriot-Watt University, Edinburgh, UK.
E-mail addresses: morteza.aminnaji@championx.com (M. Aminnaji), a.jahanbakhsh@hw.ac.uk (A. Jahanbakhsh).

https://doi.org/10.1016/j.energy.2024.131580
Received 27 January 2024; Received in revised form 1 April 2024; Accepted 6 May 2024
Available online 7 May 2024

potential advantages of CO_2 hydrates for long-term storage and reviews their formation in geological formations. It also explores the application of CO_2 injection, with a focus on CO_2-rich injections into hydrate reservoirs. The analysis highlights the advantages of utilizing CO_2 hydrates for both storage and gas recovery from these reservoirs. Particular attention is also given to the understanding of fluid flow and mechanical properties of gas hydrate reservoirs, specifically in relation to CO_2 hydrates within porous media. A review is also conducted on several crucial field tests within the domain of CCS, focusing particularly on gas hydrates and recent studies investigating the stability of CO_2 hydrates.

Finally, as the focus is to narrow onto the promising avenue of hydrate-based technologies in-depth exploration of CCS, an outlook and perspective that underscores the significance of hydrate-based CCS are presented.

2. CO_2 hydrate flow assurance

CO_2 is usually transported from the carbon capture centre via a pipeline and injected into the storage site. While CO_2 transportation is the least costly part of CCS (carbon capture cost is more than 50 % of CCS cost [1]), it needs more planning, flow assurance, pipeline integrity, and suitable design [2–4]. While Svensson et al. (2004) showed that pipelines could be an option for CO_2 transportation [5], other studies investigate CO_2 transportation cost [6–9].

Transportation of single-phase CO_2 (liquid or supercritical) is preferred due to the problems associated with two-phase flow [10]. CO_2 should be transported at a high-density condition (liquid or supercritical state) to prevent bubble formation [6]. The critical pressure and temperature of pure CO_2 are 7.38 MPa and 31.1 °C respectively. So, if the temperature is above the critical temperature (in most locations during the summer [6]), any pressure drops that result in pressure below 7.38 MPa trigger the formation of CO_2 bubbles. It is highlighted that the minimum pressure for CO_2 transportation should be higher than the critical pressure (7.38 MPa) to prevent two-phase mixture flow [6]. Fig. 1 shows Temperature-entropy (T-S) diagram for CO_2 that identifies liquid and vapour regions.

The presence of impurities can also cause a two-phase flow and increase the pressure drop [11]. In addition, dynamic simulation of CO_2 transport in the pipeline shows that some circumstances (e.g., shut-down and pipe cooling) can cause the formation of a two-phase mixture [12]. Nevertheless, the phase envelop and thermophysical properties of CO_2 streams significantly influence the pipeline design for CO_2 transportation that should be cost-effective [13] and safe for normal operation [14].

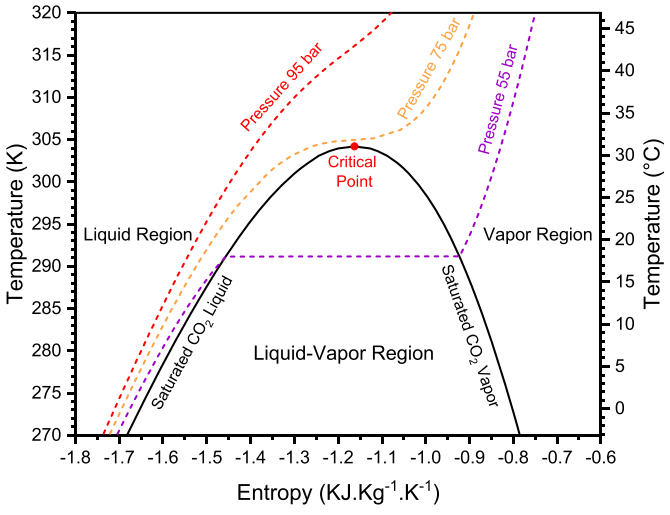

Fig. 1. CO_2 Temperature-entropy (T–S) diagram predicted by PVTsim. Note: the value of entropy depends on the reference state.

Pipeline design, construction, and operation are the main three phases for CO_2 transportation that have been investigated in other studies [15–19]. While there are some thermodynamic challenges for CO_2 pipeline design [20] and a great deal of considerations should be undertaken for CO_2 transportation [21], this section only reviews the fundamental flow assurance challenge related to CO_2 transportation focusing on CO_2 hydrate.

2.1. CO_2 hydrate flow assurance

Hydrate Risk is considered as the flow assurance problem that needs to be assessed for CO_2 transportation [22–24]. Kvamme et al. investigated the upper limit of water content in dense CO_2 during pipeline transportation to prevent hydrate formation [25]. They concluded that water adsorption on rusty pipeline walls increases CO_2 hydrate formation risk. They also examined different hydrate formation routes for transportation of dense CO_2 with water and some impurities such as hydrogen sulfide, methane, argon, and nitrogen [25,26].

CO_2 stream is practically transported under the supercritical condition using the pipelines that need to be buried in the land due to safety [27,28]. Accordingly, the properties of surrounding soil (e.g., temperature and conductivity) influence the CO_2 pipeline operation [29] which can induce hydrate formation risk. Hydrate formation risk under the transient condition in the buried CO_2 pipeline was investigated for shut-in, start-up, and rapid depressurization [30]. It is pointed out that hydrate formation risk depends on soil conductivity which has a higher risk in medium and high soil conductivity [30]. There is also always a risk of hydrate formation during the start-up and shut-in conditions if the CO_2 stream is not dehydrated [30].

Operating conditions can also enter to the hydrate stability zone during CO_2 injection into geological storage. A typical schematic diagram of CO_2 hydrate formation risk in the well injection for CO_2 geological storage is shown in Fig. 2. Wang et al. investigated gas hydrate flow assurance problem during deep-water operation and developed a model for flow assurance design and optimization [31]. A practical model was also developed by Zerpa to design the flow assurance strategies considering the hydrate formation, dynamic aggregation, and transportability in the pipelines [32]. A transient simulation model for hydrate prediction and formation in the pipeline was also investigated by numerous studies [33–37].

Heat transfer, pressure drop, and flow characteristics of CO_2 hydrate mixture have been also investigated [35,38–41]. Prah and Yun pointed out that the continuous CO_2 hydrate formation strongly depends on the temperature difference between CO_2 hydrate mixture and surrounding soil [40]. They indicated that the pressure drop and heat transfer coefficient for CO_2 hydrate mixture in the buried pipeline can be in the range

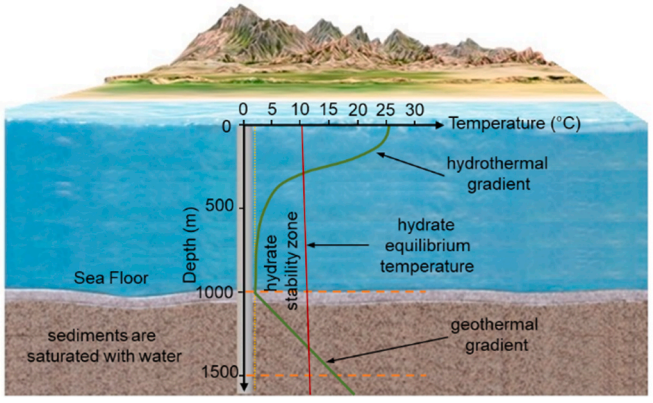

Fig. 2. Typical schematic diagram of CO_2 hydrate formation risk in the well injection. 75 bar is assumed at the wellhead for the prediction of CO_2 hydrate equilibrium temperature.

of 101–996 KPa and 54–2883 W m^{-2} K^{-1} respectively [40]. A reduction in heat transfer coefficient with increasing of CO_2 hydrate was reported by Park and Yun [42]. Oignet et al. investigated the convective heat transfer coefficient of CO_2 hydrate mixture (0–14 % hydrate fraction) and reported that it is 2.5 times higher than that for liquid water [43]. De Koeijer et al. also investigated heat transfer, impurities, depressurization, and the model for hydrate formation for CO_2 transportation [44]. The heat transfer for the gas hydrate mixture for CO_2-Ar and CO_2–He in a continuous flow reactor was also investigated by Yang et al. [45]. While Yang et al. concluded that high fluid velocity increases the mass and heat transfer in the continuous hydrate flow reactor [45], Prah and Yun showed that CO_2 hydrate particles are intended to settle down even at high velocity conditions by modelling using COMSOL [39].

The discussion on CO_2 hydrate flow assurance highlights that it is a technical discipline that needs to be considered for continuous CO_2 transportation. Accordingly, the challenge of induced CO_2 hydrate needs an understanding of the dehydration requirements for CO_2 stream, CO_2 hydrate slurry flow, CO_2 hydrate blockage, and inhibition method to prevent hydrate formation as discussed in the following subsections.

2.1.1. *Water content and its effect on CO_2 hydrate formation*

Accurate prediction of pipeline conditions that lead to hydrate formation is a complex endeavour. Kvamme et al. used a modified phase field theory (PFT) to analyse the thermodynamics and the kinetics formation of CO_2 hydrate to determine the most probable transition of hydrate phase [46]. They concluded that CO_2 hydrate formation is thermodynamically feasible above a certain limit of water concentration.

The CO_2 streams may have various impurities such as moisture, therefore, dehydration and reducing the water dew point is one of the options to prevent CO_2 hydrate formation. Hydrate equilibrium temperature significantly depends on water content in the absence of free water phase, i.e., the hydrate phase boundary shifts to the lower temperature and higher pressure by reducing the water content. While significant works have been advocated to study the CO_2 hydrate in the presence of free water phase, there are limited data on equilibrium CO_2 hydrate dissociation point in the absence of free water.

The hydrate equilibrium temperature of CO_2 in the absence of free water could be determined by measurement of water content in the vapour or liquid CO_2 phase in equilibrium with hydrate. In this method, a small fraction of water is initially injected into the cell at a temperature well above the hydrate formation temperature. The water content of vapour or liquid CO_2 phase is then measured at different temperatures by the stepwise temperature reduction (pressure is kept constant by adjusting the volume). Following this stepwise temperature reduction, the temperature is decreased significantly to convert all water to hydrate at a high subcooling temperature. The water content of vapour or liquid CO_2 phase is then measured by the stepwise increase of temperature once it reaches the equilibrium. The water content is then plotted as a function of temperature; and the hydrate equilibrium dissociation temperature can be determined by the intersection of water content curves from step-heating and step-cooling points as shown in Fig. 3.

Fig. 3 shows an example of water content in CO_2-rich liquid with 1100 ppm mol water as a function of temperature at 8.89 MPa. While the water content remains constant outside the hydrate stability zone (all water is dissolved in the CO_2 phase), it exponentially increases with temperature inside the hydrate region due to the increasing of water vapour pressure in the hydrate phase and decreasing of hydrate fraction [47]. This method was used by Chapoy et al. [47] and Youssef et al. [48] to measure the CO_2 hydrate equilibrium temperature without free water.

As discussed, the hydrate dissociation point in the absence of free water notably depends on the water content. Therefore, accurate prediction of water content in the vapour/liquid CO_2 in the presence of hydrate is essential to assess the dehydration requirement to prevent CO_2 hydrate formation. An accurate model for the prediction of CO_2

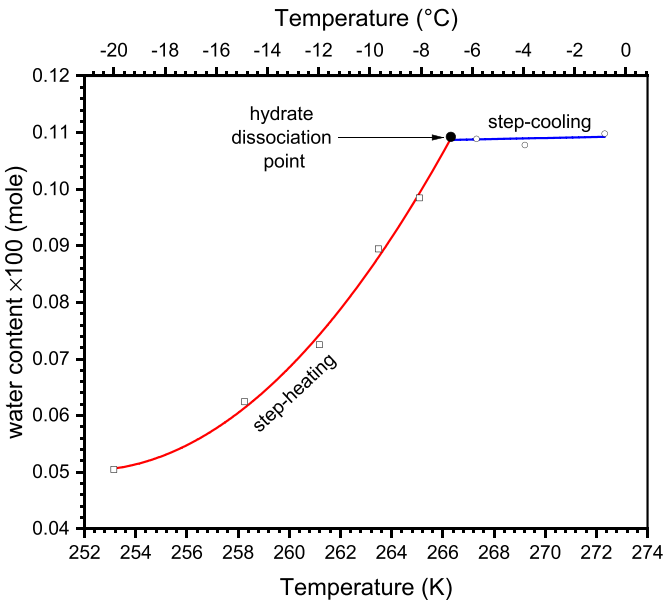

Fig. 3. An example of water content in CO_2 liquid with 1100 ppm_{mole} water as a function of temperature at 8.89 MPa to determine hydrate equilibrium point without free water. Data is taken from Chapoy et al. [47].

hydrate in the absence of free water requires the highly precise prediction of water content. Consequently, there have been numerous research investigated the water content in the CO_2-rich fluid in equilibrium with hydrate [49–53]. A large discrepancy in the water content of CO_2-rich phase in the hydrate stability zone was reported due to the metastable of the hydrate phase, slow process of hydrate formation, and presence of an unexpected phase [53]. However, all experimental data demonstrate a sharp discontinuity in water content in the CO_2 rich phase in equilibrium with hydrate (or liquid water) when the CO_2 phase is changed from vapour to liquid [50,54–57]. The equilibrium water content in the CO_2-rich phase increases in step change when the CO_2 phase is changed from vapour to liquid. It is reported that the pressure has very little effect on the water content in the liquid CO_2 in equilibrium with CO_2 hydrate [52].

Fig. 4 also shows the CO_2 hydrate-vapour equilibrium at different water contents. It indicates that the hydrate phase boundary shifts to a lower temperature and higher pressure (in the absence of free water) as the CO_2 stream is dehydrated. This determines the amount of dehydration requirement to prevent hydrate formation. It has been noted in some studies that the CPA equation of state combined with classical Platteeuw and van der Waals model can properly predict the hydrate phase boundary of CO_2 in the absence of free [47,48].

2.1.2. *CO_2 hydrate inhibition*

Chemical injection is the most popular techniques to prevent hydrate formation. Thermodynamic hydrate inhibitors (THIs) and low dosage hydrate inhibitors (LDHIs) (kinetic hydrate inhibitors (KHIs) and anti-agglomerants (AAs)) are two types of chemicals for hydrate inhibition. These chemicals, particularly focused on CO_2 hydrate inhibition, are discussed in this section.

(a) Thermodynamic hydrate inhibitors (THIs)

THIs (e.g., mono-ethylene glycol (MEG), methanol, and ethanol) disrupt the hydrogen bonding and reduce the hydrate equilibrium temperature at a particular pressure [74]. Specifically, when considering ethanol as a THI, powder X-ray diffraction and molecular dynamics simulations demonstrated that in the CO_2 + ethanol + water, both CO_2 and ethanol can act as guest formers in hydrate lattice. The

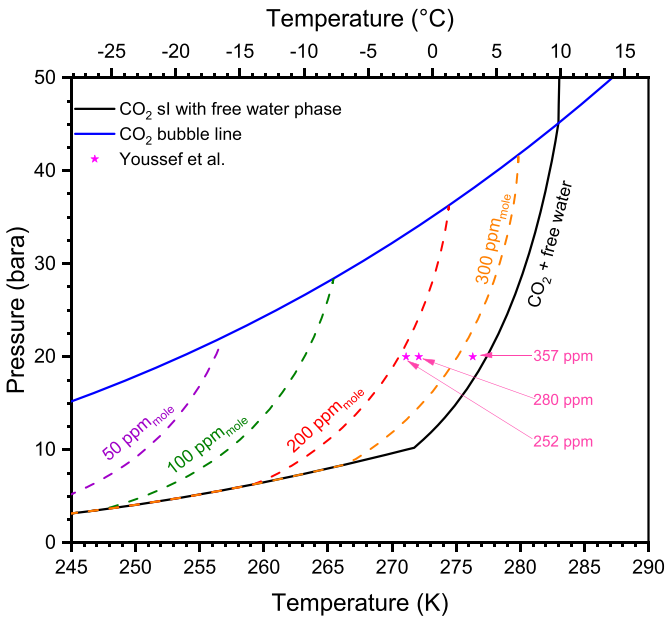

Fig. 4. CO_2 hydrate phase boundary at different water contents predicted with PVTsim. A few experimental data from Youssef et al. [48] are added for comparison.

results showed different hydrate lattices, with a lattice constant of 1.8577(5) Å at 113 K for the system with ethanol, which is larger than the pure CO_2 lattice constant of 11.8434(8) Å [58].

Fig. 5 shows various THIs that have been studied for CO_2 hydrate inhibition. Some organic solvents such as dimethyl sulfoxide have also THIs inhibitory effect on CO_2 hydrate [59]. In addition to alcohol and glycol, ionic salts such as NaCl can act as THIs. The inhibition and induction time of CO_2 hydrate are influenced by salts i.e., while salts can act as THIs, they have some effect on CO_2 hydrate nucleation and growth. Farhang et al. investigated the effect of sodium halides (NaF, NaCl, NaBr, and NaI) on the CO_2 hydrate kinetic and concluded that while salts are known as THIs, they can increase the kinetics formation of CO_2 hydrate at low concentration (e.g., 50 mM) [75]. In contrast, it is reported that CO_2 hydrate growth rate in 3.5 % electrolyte solution of NaCl, KCl, $CaCl_2$, and $MgCl_2$ is slower than in deionized water [76].

Some ionic liquids (ILs) also have THIs properties. For example,

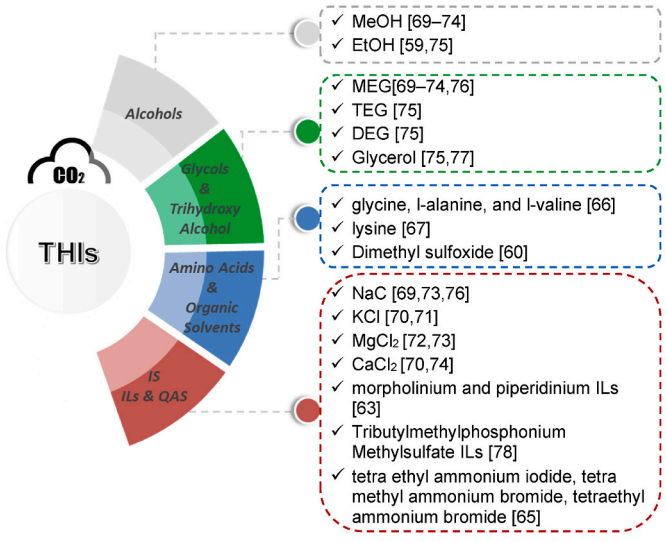

Fig. 5. Thermodynamic hydrate inhibitor available in the literature for CO_2 hydrate inhibition [58–73]

morpholinium and piperidinium ionic liquids have THIs inhibition effect on CO_2 hydrate [60]. Cha et al. showed that smaller anionic species in morpholinium and piperidinium ionic liquids have a better inhibition effect [60]. The inhibition performance of various ions on CO_2 hydration inhibition has been summarised by Liu et al. [77]. In addition to ILs, quaternary ammonium salts (QAS) have also THI properties. For example, the THI properties of three QAS (tetra ethyl ammonium iodide, tetra methyl ammonium bromide, and tetraethyl ammonium bromide) with and without MEG were reported for the CO_2 hydrate [61]. Some amino acids may also act as THIs. For example, glycine, L-alanine, and L-valine show THIs inhibition properties in the CO_2 hydrate system [62]. Manner et al. also studied the effect of lysine as amino acid on CO_2 hydrate and showed that 10 wt% lysine can reduce the equilibrium temperature of CO_2 hydrate by 1.49 K [63]. However, some amino acids have some properties to increase gas uptake capacity and kinetics during gas hydrate formation [78].

(b) Kinetic hydrate inhibitors (KHIs)

KHIs are water-soluble polymers that can increase the induction time by inhibiting of hydrate nucleation and preventing catastrophic hydrate growth [79]. Molecular dynamic simulation shows that KHIs affect the water molecule arrangement and increase the induction time by the interaction between KHI molecules and hydrate nuclei surface [80,81]. It is proposed that KHIs reduce the supersaturation of gas and reduce the gas migration to the hydrate nucleus which results in hydrate growth inhibition [81]. Induced hydrate dissociation by KHIs inside hydrate stability zone has been also reported [82,83]. It has also shown that KHIs can inhibit the growth of pre-formed hydrates [83]. In the past decade, significant advances have been achieved in both developments of KHIs polymers [84,85] and biodegradable KHIs [86–88].

Some poor biodegradable commercial KHIs, e.g., poly(vinylpyrrolidone) (PVP) [89] and polyvinylcaprolactam (PVCap) [90], can inhibit the CO_2 hydrate nucleation and growth. Due to the low biodegradation of these KHI polymers, various eco-friendly KHIs such as ILs [91–93], QAS [94], and amino acids [95] have been also studied for CO_2 hydrate inhibition. It has been showed that those amino acids that have shorter alkyl chains can better inhibit CO_2 hydrate [96]. Another study also showed that the amino acids with lower hydrophobicity have better KHIs properties for CO_2 hydrate inhibition [96]. In fact, the water structure for the formation of hydrate cavity is disrupted by amino acids that have hydrophilic or electrically charged alkyl chains [97]. Some biodegradable polymers such as pectin and starch were also investigated for CO_2 hydrate inhibition [90,98]. Some ILs and QAS have been identified as dual functional hydrate inhibitors that show both KHIs and THIs properties. Khan et al. investigated the dual functional hydrate inhibitor properties of tetramethyl ammonium hydroxide, tetraethyl ammonium hydroxide, tetrapropyl ammonium hydroxide, and tetrabutyl ammonium hydroxide [99]. Fig. 6 shows various KHIs studied for CO_2 hydrate inhibition. These KHIs generally are divided into four categories: non-biodegradable polymers, green polymers and amino acids, ILs, and QAS.

Inhibitor effect of KHIs on CO_2 hydrate is significantly influenced by subcooling temperature (i.e., a temperature difference between operating condition and hydrate equilibrium). KHIs can induce different inhibition regions as a function of subcooling temperatures including complete inhibition region (CIR), slow growth region (SGR), and rapid growth region (RGR), i.e., these regions which are induced by crystal growth inhibition intensity of KHIs are identified by crystal growth inhibition (CGI) method [101,102]. Moreover, the hydrate growth rate may also affected by stirring RPM in the laboratory experiments [103]. Noticeably, the inhibition performance of KHIs on CO_2 hydrate and the induction time increase with the chemical dosage [89,100]. The CO_2 consumption through hydrate formation is another factor that is influenced and could be decreased by inhibition additives. Lie et al., summarised CO_2 gas consumption in the presence of various additives that

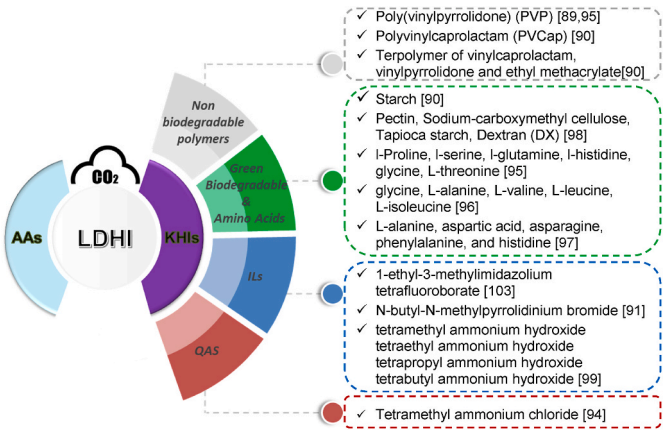

Fig. 6. Kinetic hydrate inhibitor available in the literature for CO_2 hydrate inhibition [89–91,94–100].

are reported in the literature [77]. KHIs also show some synergistic effect when they combined with THIs [74,104]. The synergistic effect of diethylene glycol and glycine has been shown for CO_2 hydrate inhibition [105].

(c) Anti-agglomerants (AAs)

The KHIs performance is subjected to subcooling temperature and may not inhibit the hydrate nucleation or growth at high subcooling temperature. Therefore, AAs (mostly oil-soluble surfactants) can be employed to avoid hydrate agglomeration/blockage [106]. Various mechanisms have been proposed to reduce hydrate agglomeration tendency by AAs. In the most common mechanism, AAs bind to the hydrates through their hydrate-philic head penetration to the hydrate cavities and make the oil-wet hydrate crystals by their hydrophobic tail [107,108]. In this mechanism, the hydrate agglomeration tendency is reduced by disruption of the capillary water bridge that can link up the hydrate crystals [109]. In another word, AAs can reduce the interfacial tension which results in decreasing in capillary forces and attraction forces between hydrate crystals [110]. It was also reported that functionalized nanoparticles could prevent hydrate agglomeration [111]. For example, silica nanoparticles show anti-adhesive effect on gas hydrate particles [112,113].

Notwithstanding the mechanisms, AAs form a hydrate slurry flow in the pipelines and various studies were done to evaluate CO_2 hydrate slurry in the presence of AAs (Fig. 7). Therefore, the rheology of hydrate slurries in the presence of various AAs has received considerable attention [114,115], and different rheology models have been proposed for hydrate slurry flow [116]. These mechanisms that are suggested for

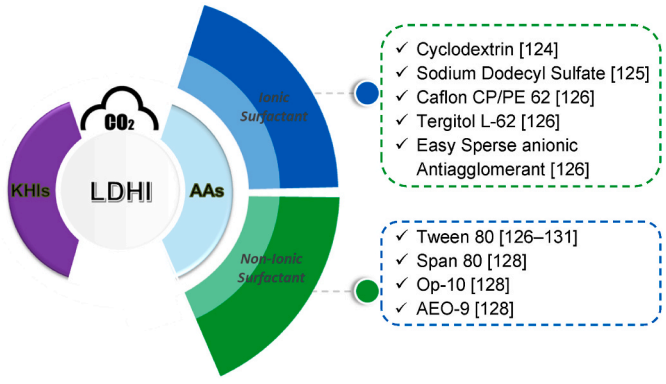

Fig. 7. Anti-agglomerants available in the literature for CO_2 hydrate inhibition [124–131]

AAs indicate the crucial function of oil phase and water cut. However, in the absence of oil phase, AAs can also prevent hydrate agglomeration [117,118], (i.e., hydrophobic tails of AAs pass through the hydrate particle surface and prevent agglomeration [119]). Some other factors, including concentration [120], gas composition [121,122], alkyl tail chain length of AAs [123], and salinity [117] can also affect AAs performance.

2.1.3. CO2 hydrate slurry flow and blockage

CO_2 transportation in the hydrate slurry form reduces the required energy for transportation and prevent hydrate blockage. Moreover, the application of CO_2 hydrate slurry for refrigeration has inspired many researchers to investigate the flow characteristic and rheological properties of CO_2 hydrate slurry. Oignet et al. [125], Delahaye et al. [126,132], Jerbi et al. [133], investigated the rheological properties (e.g., viscosity, shear stress, rheograms) of CO_2 hydrate slurry through the flow loop and tank reactor.

Hu et al. [134] experimentally investigated the flow characteristics of CO_2 hydrate slurry such as viscosity and density that are increased with solid mass fraction. They showed that CO_2 hydrate crystals has a slightly influence on the increasing of viscosity for the range of 1.59 %–28 % solid mass fraction [134]. Moreover, adding AAs makes the hydrate slurry and changes its rheological properties. Wu et al. experimentally showed that while CO_2 hydrate blockage occurred easily in the water, adding Tween-80 prevented hydrate blockage [131]. Moreover, while AAs significantly improve the flow of CO_2 hydrate slurry, they affect the hydrate slurry density, kinetics of hydrate formation, and hydrate fraction [127]. Lv et al. showed that increasing of surfactant hydrophile−lipophilic balance (HLB) of AAs results in decreasing of apparent viscosity of CO_2 hydrate slurry [128].

The sheer-thinning behaviour (similar to pseudoplastic fluid) was observed in the CO_2 hydrate slurry in the presence of AAs [128]. Similarly, Wu et al. showed that while the slurry form of CO_2 hydrate in the pure water is a dilatant fluid (shear-thickening behaviour), adding Tween-80 makes CO_2 hydrate slurry to a pseudoplastic fluid (shear--thinning behaviour) [131]. Shear-thinning behaviour observed by adding AAs is the main factor to form the CO_2 hydrate slurry and prevent hydrate blockage, i.e., moving from dilatant fluid to pseudoplastic fluid by adding AAs [131]. Moreover, increasing of SDS concentration reduces the yield stress of CO_2 hydrate slurry (i.e., shear-thinning pseudoplastic behaviour) [135]. Increasing the hydrate fraction also makes the hydrate slurry to have more non-Newtonian behaviour with decreasing of apparent viscosity. Fu et al. experimentally showed CO_2 hydrate slurry as a shear-thickening power law fluid [136].

Prah and Yun [130] identified three different flow regimes (homogeneous, heterogeneous, and bedding flow) for CO_2 hydrate slurry in the flow loop, which depends on hydrate fraction. They showed two different regions (active formation and less active formation) for CO_2 hydrate formation in the presence of AAs [130]. Prah and Yun [129] also investigated the pressure, temperature, density, and flow rate of CO_2 hydrate slurry in the scaled-up flow loop in the presence of Tween 80. They suggest that CO_2 hydrate slurry can be transported over a long distance in the presence of appropriate AAs [129].

Despite the advantages of CO_2 transportation in the form of hydrate slurry, there is always a risk of hydrate blockage in the pipeline [137–142]. Therefore, understanding of CO_2 hydrate accumulation and blockage mechanism is crucial to prevent the severe economic impact on the operation. The CO_2 hydrate blockage is very likely to occur after the onset of CO_2 hydrate formation even at small hydrate fraction [143]. It is proposed that CO_2 hydrate blockage may occur by sticking and growing of CO_2 hydrate particles on the pipe wall during four stages: induction time, formation of CO_2 hydrate layer, thickening of hydrate layer, and hydrate blockage [143]. Lv et al. experimentally investigated the effect of flow rate, pressure, and pump restarting on the CO_2 hydrate blockage in a flow loop using Focused Beam Reflectance Measurement [144]. They showed that while CO_2 hydrate blockage tendency increases with

pressure, the time required for hydrate blockage increases with flow rate [144]. They also showed that pump restarting after CO_2 hydrate blockage makes the problem worse [144]. Shi et al. also showed that the rapid restart process after CO_2 hydrate blockage can increase hydrate regrowth resulting in secondary blocking [143]. The Chord Length Distribution of CO_2 hydrate particles shows that hydrate particle coalescence causes the hydrate blockage which is time dependent [144].

3. CO_2 hydrate: geological storage

3.1. CO_2 hydrate in sediment

The initial stages of CO_2 sequestration in reservoirs typically involve evaluating geologic formations, including factors such as volume, injection rate, capping mechanisms, and capacity characteristics. These evaluations serve as crucial phases in understanding the feasibility of CO_2 storage in reservoirs. While the primary risk associated with every CCS project is CO_2 leakage from storage sites [145–147], multiple capping mechanisms may stop the CO_2 plume from migration. One of these mechanisms is CO_2 hydrate formation which is induced by the thermodynamic conditions in sediments and can stop CO_2 leaks through the top seal. This suggests that CO_2 hydrate self-sealing mechanism can be used for CO_2 storage in permafrost. The CO_2 hydrate's ability to preserve itself can also aid in lowering the danger associated with the geological setting for CO_2 sequestration [148].

Chemical additives have a significant effect on hydrate formation in sediment. While they have minimal effect on the properties of water, they can improve hydrate formation by approximately 50 % (0.15 wt% SiO_2) and 25 % (0.05 wt% SDS) compared to pure sea water [149]. The in-situ magnetic resonance imaging (MRI) demonstrated that the rate of hydrate dissociation in sediments-carrying organisms can be four times faster for the sample with 23 % saturation than for the sample with 38 % saturation [150]. CO_2 hydrate dissociation rate can be also decreased by 0.12, 0.12, and 0.16 mMole.min^{-1} compared to pure water with silica gel powder, SDS, and their mixture respectively [151]. When the effects of acid-soluble organic materials, such as lignin and protein/amino sugars, were examined, it became clear that their presence on the seafloor would kinetically enhance hydrate formation [152]. Hydrophilic silica nanoparticles was also used for CO_2 storage as a highly porous CO_2 hydrate structure, i.e., they provide numerous CO_2 hydrate nucleation sites [153].

The difference in saturation between primary and secondary hydrate formation in porous media results in two types of hydrate: hydrate filled inside the pores (filling model) and hydrate adhering to the surface (coating model). The free gas in large pores preferentially synthesises hydrate, which fills the pores during hydrate formation. This process creates a "hydrate layer" that blocks CO_2 from entering the porous medium. The "hydrate layer" also reduces CO_2 hydrate formation. Wen et al. (2021) [154] stated that the formation of hydrate in seabed sediments mainly consumes water in large pores, followed by a diffusion limitation process in which the hydrate layer acts as a mass transfer barrier, making it difficult for water in small pores to participate in the reaction. In secondary formation, CO_2 gas can enter all pores to produce hydrate, therefore the hydrate accumulates on the porous medium particles. The formation of CO_2 hydrates alongside frozen quartz sands demonstrated how smaller particle sizes could boost gas storage capabilities [155].

3.2. CO_2 hydrate self-sealing

One critical aspect of geological CO_2 storage is the caprock integrity for safe CO_2 storage [156–158]. The self-sealing mechanism through CO_2 hydrate formation is a process that not only ensures the caprock's integrity but also enhances the overall effectiveness and security of geological CO_2 storage. This natural process plays an important role in the seal of the geological reservoir and supporting the long-term stability of the storage site. As shown in Fig. 8, if CO_2 is stored below the gas hydrate stability zone, the leaked CO_2 (through vertical migration of CO_2) can form hydrate in the CO_2 hydrate stability zone resulting in permeability reduction. It is pointed out that the temperature below 5 °C at higher hydrostatic pressure (e.g., few hundred meters of water) could initiate CO_2 hydrate formation in the gaps of rock to prevent CO_2 leakage [159]. Another study indicated that CO_2 hydrate and storage in the cool underground sediment enhances the CO_2 trapping which have some advantages including physical, chemical, and mineralogical processes [160].

Tohidi et el. showed CO_2 hydrate formation in synthetic porous media through visual observation without the presence of a free-gas phase. They showed hydrate formation in the centre of pore spaces providing potential cementing effect and reducing permeability [161]. Tohidi et el. also showed the upward migration of CO_2 into the hydrate stability zone can form hydrates and provide a secondary safety factor to prevent CO_2 leakage [162]. They showed that formation of CO_2 hydrates significantly reduced the CO_2 diffusion rate by three orders of magnitude [162]. A pore-filling hydrate morphology is suggested as a mechanism to reduce the rock permeability even at low water saturation (36 %) [163]. It has been showed that temperature and salinity affect the hydrate induction time in the sediments [163]. However, experimental works showed that CO_2 hydrates are sufficiently stable inside the deep oceanic saline sediments (3.5 wt% NaCl) [164]. The CO_2 hydrate stability in the oceanic sediments was also confirmed through a laboratory-scale high-pressure reactor [165]. Moreover, Gauteplass et al. experimentally showed that the integrity of the CO_2 hydrate seal is strongly affected by fluid-rock interactions and initial water distribution [166]. Their research demonstrated that CO_2 leakage rate is ten times slower in sandstone compared to limestone, through CO_2 hydrate formation. The presence of CO_2 may also change fluid-rock interactions such as the degree of swelling and transport properties of clay mineral–water–CO_2 systems [167].

Monte Carlo study also showed coexistence of CO_2-free gas, CO_2 hydrate, and dissolved CO_2 in the hydrate stability zone [168]. In this three-phase zone, the entrapped CO_2 bubble due to the capillary pressure reduce the effective permeability [168]. The coexisting of CO_2 bubbles and hydrates to reduce the permeability has been also confirmed in another study [169].

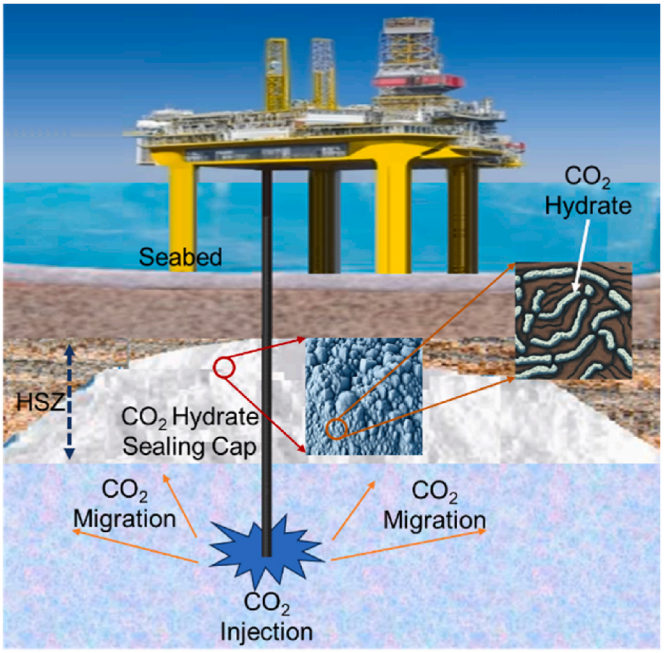

Fig. 8. CO_2 hydrate self-sealing mechanism in the hydrate stability zone.

3.3. CO_2/CO_2-rich injection into gas hydrate reservoirs

Methane extraction from hydrate reservoir remains largely unexplored due to low production efficiency [170,171]. Applying chemical, thermal stimulation, and pressure reduction may not be a practical options for production from hydrate reservoir [172,173]. In contrast, CH_4–CO_2 swapping by injection of CO_2 or CO_2–N_2 mixture into hydrate reservoir allows CH_4 recovery and CO_2 storage at the same time as shown in Fig. 9 [174–176]. CO_2 hydrates are more thermodynamically stable than CH_4 hydrates, therefore they spontaneously exchange [177]. Swapping between CH_4 and CO_2 retains adequate hydrates and stabilizes hydrate-bearing sediments [178,179]. The process of CH_4–CO_2 exchange was also confirmed by injection of liquid CO_2 through methane hydrate sediment [180]. MRI imaging also approved the CO_2/CH_4 substitution in sandstone core plugs [181]. Furthermore, field simulation was used to evaluate the replacement process of CH_4 hydrate with CO_2 when the CO_2 liquid is present [182]. The possibility of CO_2 hydrate nucleation and replacement in the CH_4–CO_2 sweeping process was also confirmed through a theoretical approach by using the density functional theory (DFT) coupled with the reference interaction site model (RISM) [183]. Qta et al. [184] employed Raman spectroscopy to study liquid CO_2 and CH_4 replacement in the hydrate. They found that CH_4 molecules may fit into relatively narrow gaps. Kvamme et al. [185] combined MRI and Phase Field Theory to create the model needed to visualize the conversion of CH_4 hydrate into CO_2 hydrate in the sandstone. These techniques (MRI and Phase Field Theory) were also used to identify kinetics of CO_2 hydrate formation in porous media [186].

The replacement of CH_4 hydrate with CO_2 is controlled by the chemical potential of gas molecules, mass transfer, and hydrate history [188]. The efficiency of CO_2 replacement for extracting natural gas hydrates is influenced primarily by injection rate and total amount of injected CO_2, along with the thermodynamic conditions [147]. It was also proposed that low-concentration and biocompatible hydrate inhibitory chemicals could induce CH_4 recovery and confine CO_2 in hydrate consortiums [189]. Inhibitors like NaCl may also help to accelerate the process of replacing CO_2, and improve the prospects of diverting thermodynamic equilibrium conditions outside the CH_4 hydrate stability zone [190].

Molecular dynamic simulation shows that this process is followed by dissociation of methane hydrates and then formation of an amorphous CO_2 hydrate layer, i.e., the formation of CO_2 hydrate as the amorphous layer results in a constraint on the mass transfer [188]. However, while some studies show the transition of guests between adjacent cages through their faces only by destroying their water structure, density functional theory shows a direct transition mechanism [191]. In another study, molecular dynamics simulation shows that CO_2 promotes early nucleation of CH_4 bubbles during the methane hydrate decomposition [192]. This process leads to form mixed CO_2–CH_4 bubbles with a high concentration of CO_2. This CO_2 stabilizes the interface by reducing surface tension and lowering the bubble's critical size, facilitating methane hydrate decomposition.

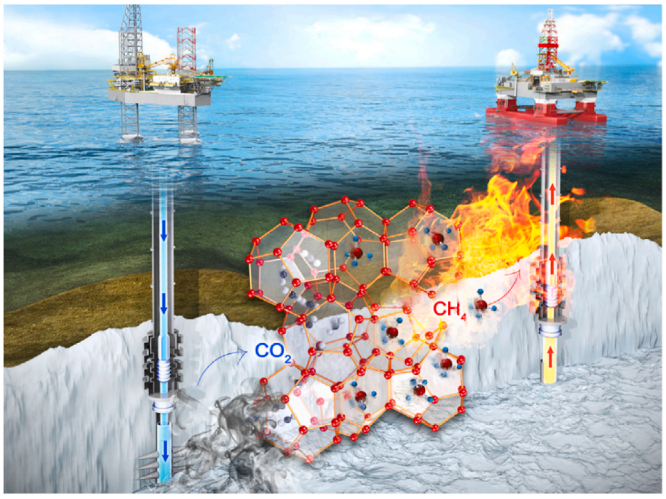

Fig. 9. CH_4–CO_2 swapping or exchange by CO_2 injection in hydrate reservoir, allowing CH_4 recovery and CO_2 storage. Reprinted with permission of Elsevier [187].

A high occupancy ratio of large to small cages of methane sI hydrate has been reported in the sediment which might affect CH_4–CO_2 swapping [193]. The morphology of hydrate crystals may also affect this process. The crystal morphology of the CH_4 + CO_2 hydrates is affected by the composition in the liquid phase, i.e., it changes from polygons to sword-like as subcooling temperature increases [194].

CH_4–CO_2 swapping uses little energy and produces little water, making it competitive with other exploitation methods [195,196]. Nevertheless, the commercial utilization of CH_4–CO_2 swapping is hindered by the limitation imposed by mass transfer constraints, leading to a slow process [197,198]. Experimental data showed that CH_4 might be selectively replaced with CO_2, with an estimated CH_4 average distribution coefficient of 2.5 between gas and hydrate states [199]. The hydrate kinetics can also be improved by adding water infusions during CO_2 sequestration in hydrate reservoir [200]. Moreover, thermal stimulation and higher sediment hydrate fraction can increase the process methane hydrate replacement with CO_2 [179].

After the replacement process, the 13C NMR spectroscopy showed the existence of CH_4 in the tiny cages of structure II, but only a small number were found in the hydrate of structure I [201]. The quantity of CO_2 captured during the hydrate phase depends on the reservoir's temperature, pressure, and hydrate saturation. After dissociation, gas composition examination of the hydrate showed a significant amount of CO_2, which is moderately affected by temperature [202]. Another important factor is the pressure of the injected CO_2. For instance, the higher CO_2 injection pressure results in higher replacement rate and CH_4 recovery [201].

There may be some unfavourable effects of this phenomenon. For instance, the recovery of CH_4 can cause shrinkage, whereas the injection of CO_2 can cause swelling and permeability reduction [203]. Furthermore, even though researchers have verified the CO_2/CH_4 exchange in the pore space and the reservoir's mechanical stability for a period of 24 h, the rate of a gas exchange over 24 h could not be very high [204]. Therefore, hydrate stability in porous media should be experimentally determined, i.e., optical pore-scale observations can be used as a procedure to map hydrate transition and hydrate stability zones in the sediments [205].

Additionally, CO_2+N_2 mixture is preferred over pure CO_2 injection into the hydrate reservoirs [206]. CH_4 recovery from hydrate reservoir by flue gas injection (CO_2 + N_2) is highly affected by its composition and pressure [207–209]. The composition of injected gas has a minor impact on displacement efficiency at high flow rates [210], whereas semi-continuous gas injection significantly improves recovery of CH_4 when CO_2 levels are low [211]. The molecular dynamic simulation also showed that the higher ratio of CO_2:N_2 increases the nanobubbles nucleation which may affect the replacement process of CH_4 with CO_2 and the structural ordering of water molecules [212]. A study showed that the maximum concertation of N_2 in the CO_2–N_2 mixture should be around 30 mol% [172]. Saeidi et al. also showed that the methane production increases by injection of CO_2–N_2 mixture rather than injection of pure CO_2 into the CH_4 hydrate in the sediment, i.e., the maximum release of CH_4 was observed at 20 mol% N_2 in the flue gas [213].

3.4. Mechanical properties of gas hydrate in sediment

Gas hydrates naturally exist in the oceanic sediments and permafrost locations [214]. Gas hydrates are stable in nature, with methane as the main gas, along with traces of other gases such as ethane, CO_2, and H_2S

[215–219]. Approximate global gas hydrate inventory is estimated to be around 1.8 × 103 Gt of carbon, which is equivalent to a methane volume of 3.0 × 1015 m^3 [171]. The substantial quantities of carbon present have led to the recognition of methane hydrate as a prospective energy source and a geological hazard [220–222]. The process of gas extraction from methane hydrates (for example using CO_2 injection) has the potential to trigger various geological hazards, including subsea landslides, casing deformation, and production platform collapse [223,224]. Therefore, it is crucial to conduct a comprehensive investigation into the mechanical characteristics of hydrates sediments. However, in the context of CO_2 hydrate formation in the geological formations, understanding the mechanical assessments of hydrate-bearing sediment (HBS) based on the geotechnical testing at macroscopic and microscopic levels is important to provide insights into the stability of CO_2 hydrate in sediment. This section summarizes mechanical assessments of hydrate-bearing sediment and how some factors such as hydrate saturation, confining pressure, and sediment composition affect HBS mechanical performance.

3.4.1. HBS's mechanical behaviour

Safety assessment of methane hydrate reservoirs is essential, with particular emphasis on the analysis of their strength characteristics in the case of CO_2 or CO_2/N_2 injection. The evaluation of mechanical characteristics of sediment-containing hydrates primarily involves the utilization of two methods: the elastic property test, which is an indirect approach, and the mechanical strength test, which is a direct approach [223].

Triaxial test is one of the most common methods for mechanically assessment of hydrate-free sediment (HFS) and hydrate-bearing sediment (HBS). In this regard, the volumetric strain is the ratio of the sediment's modified volume to its initial volume. In addition, the axial strain is defined as the ratio of the sediment's changed length to its principal length. The difference between major and minor primary stress in a triaxial test is also defined as deviator stress. During the triaxial test conducted on the specimen (a sample of HBS), both normal stress and shear stress are normally applied.

In the zone where the deviator stress increases with axial strain at a slower rate, HBS deforms plastically. Although higher axial strain increases the deviator stress rate, shearing sand particles may generate more significant rotation, slippage, and rearrangement. This phase crushes and sheds the cemented sand particles around the hydrate particles. Moreover, the separated hydrate particles will keep the sand particles near to their original position [225]. The preservation of hydrate particles prevents sand particle rearrangement; thus, the particles must manoeuvre around neighbouring particles. Consequently, HBS may exhibit dilatancy [225] (dilatancy is the volume change in shear-deformed granular materials). In the hydrate-cemented cluster, wedge-shaped hydrates hardly deform, preventing sand particle rearrangement [226]. At the yielding zone, deviator stress hardly varies and may even decrease with axial strain. This disperses the hydrate-cemented cluster and disrupts the cementation structure. The shear band is the primary location of deformation [227].

Numerous triaxial testing apparatuses have been developed specifically for HBS analysing. Notably, Yamaguchi University [228,229], Kyoto University [230], National Institute of Advanced Industrial Science and Technology (AIST) [231], University of Calgary [232], and Dalian University of Technology [233,234] have made significant contributions in uncovering the macroscopic mechanical characteristics in assessing the geotechnical implications associated with gas hydrate production. X-ray CT was utilized to conduct a series of experiments aimed at elucidating the microscopic structural properties of HBS [235]. Additionally, a pressurized sub-sampling system was developed specifically for X-ray CT scanning purposes. In this study, Takeya et al. reported that hydrate, which was stored under preservation conditions that deviated from the norm, exhibited complete envelopment and stabilization due to the presence of a thin layer of ice [236]. Nevertheless, due to the challenging nature of achieving X-ray penetration under high-pressure conditions, only a limited number of mechanical studies have been conducted at the microscopic level.

Shear strength and pore pressure of sediments hold significant importance in ensuring the stability of sediments [237]. The available literature suggests a positive correlation between shear strength of sediments containing methane hydrates and several factors, namely methane hydrate saturation [231], effective confining pressure [238], pore pressure [229], and fines content [239]. Sediments containing methane hydrates also demonstrate elevated shear strength at reduced temperatures, as reported by Jiang et al. [240] and Shen et al. [241]. Furthermore, numerical simulations showed that an increase in salinity has a detrimental effect on the shear strength of HBS [242]. This decrease in shear strength can be attributed to the inhibitory effect of salinity on the formation of hydrates, as highlighted by Chen et al. [243]. However, the primary cause of macroscopic deformation in hydrate sediments is attributed to the migration or slip between individual sand grains [244].

Moreover, as the degree of deformation increases, the localized tensile/shear stresses surpass the strength threshold of the hydrate cement, thereby resulting in the inevitable occurrence of damage or failure in the hydrate cementation process [245]. In the separate studies, Ghiassian and Grozic [246] and Grozic and Ghiassian [247] performed undrained triaxial shear tests on sand containing methane hydrates. The findings of these experiments indicated that the presence of hydrates led to enhancements in the strength, stiffness, cohesion, and internal friction angle of the sediment.

Hydrates have been observed to provide cementation [248,249]. However, the dissociation of hydrates can potentially lead to a reduction in the stiffness of sediment layers [250], ("stiffness" is the sediment's early deformation resistance as seen by the deviator stress-axial strain curve's first slope). Moreover, liberation of gas and water resulting from hydrate dissociation would compromise the interparticle bonding, thereby exacerbating the reduction in the rigidity of sediments containing hydrates. Therefore, it is crucial to ensure the preservation of the rigidity of HBS to prevent geological hazards during the process of gas hydrate extraction by CO_2 injection [223].

3.4.2. Hydrate saturation effects

Sediment strength is highly affected by hydrate saturation. Iwai et al. conducted undrained triaxial tests on sandy sediments containing CO_2 hydrates [251]. Their findings revealed a positive correlation between hydrate saturation and the strength and stiffness. Sun et al. conducted undrained triaxial experiments on sand containing methane hydrate [252]. Their findings revealed a positive correlation between failure strength and both methane hydrate saturation and effective confining pressure. The effect of hydrate saturation on HBS strength has been studied by numerous researchers which are summarised by Wu et al. (2020) [253].

It has been observed that hydrate saturation has a minimum effect on the HBS strength at low hydrate saturation. This can be attributed to the formation of hydrate only on the sand particle surface with minimal interaction between adjacent sand particles. Consequently, the shear force can exceed the cementation strength of the hydrate, leading to minimal strength of the sediment [254]. In contract, at higher hydrate saturation, the presence of cementing due to pore-filled hydrates may prevent sand particle displacement and provide increased resistance to pressure. A substantial cluster of sand particles cemented by hydrates can create localized challenges for shearing. Experimental studies on triaxial compression tests for CO_2-hydrate sand have demonstrated a similar trend aligning with the discussion on the effect of hydrate saturation on the strength of HBS [255].

The significance of hydrate saturation and hydrate pore habit in relation to permeability and water retention characteristics has been well-established in previous studies [256–258]. The permeability of HBS can exhibit significant variations by several orders of magnitude, even

when the hydrate saturation remains constant [259,260]. The pore structure HBS has been determined to exhibit a pore-filling pattern through in-situ seismic analysis conducted at the Blake Ridge [261] and the Mallik sites [262], as well as wave velocity measurements performed on pressure cores obtained from the Nankai Trough [263]. Moreover, it is worth noting that most HBS created in laboratory settings tend to display pore structures characterized by either grain-coating or contact-cementing patterns. This is particularly observed when these sediments are formed under unsaturated conditions, specifically through the utilization of the excess-gas method [264].

Hydrate saturation plays a crucial role in determining the quantity of gas that can be dissociated from the hydrate. Additionally, it can have substantial impacts on the physical characteristics of the hydrate reservoir, including permeability and thermal conductivity. These factors influence the behaviour of both dissociated gas and flow of water within the reservoir. Hence, the assessment of hydrate saturation holds significant importance in determining the economic viability of industrial operations pertaining to the extraction of natural gas hydrate. Xiong et al. provided a concise discussion on the influence of hydrate saturation on the dissociation behaviours of methane hydrates within a one-dimensional experimental setup [265].

3.4.3. Confining pressure effects

Adequate confining pressure can increase HBS strength. At enough confining pressure, sand and hydrate particles may interlock more forcefully, increasing internal sediment friction. However, higher confining pressure may impede fracture development and reduce sand and hydrate mobility [228]. In triaxial tests employing on frozen HBS, HBS deviator stress shows an increase and subsequent fluctuation with increasing confining pressure [233]. Winters et al. examined the impact of pore pressure on methane hydrate bearing sandy and silty sediments under undrained shear conditions [266]. The results indicated a decrease in pore pressures for sandy sediments, while silty sediments exhibited a positive pore pressure response.

Previous studies have indicated that an elevation in effective stress can result in various consequences, such as increased deformation, reduced permeability, volumetric yield, and even particle fragmentation [267–269]. It has been observed that the complete conversion of hydrates into gas and water doesn't occur instantaneously upon reduction of pore pressure below the equilibrium state [270,271]. The process of dissociation in hydrate reservoirs involves a temporal duration from initiation to completion, with an intermediate region existing between the dissociated and undissociated areas [272]. The findings above suggest that the sediments containing hydrates in the transition zone exhibit low pore pressures and high effective stresses, accompanied by a gradual decline in saturation.

Several well-documented hydrate reservoirs, including various locations in the Nankai Trough (offshore Japan), the Gulf of Mexico, and the Krishna-Godavari Basin (offshore India), predominantly consist of sandy formations situated at depths exceeding 2000 m below the water surface [273,274]. It is anticipated that particle fragmentation is expected to take place in these regions during the process of depressurization, potentially influencing the mechanical characteristics of the sediments. Furthermore, it should be noted that the generation of fine particles, which are smaller than the pore throat, can occur as a result of particle breakage. The movement of these particles potentially cause blockages. This phenomenon has been reported in studies conducted by Uchida et al. [275], Cohen et al. [276] and Lei and Seol [277]. It is important to recognize that such occurrences can have detrimental effects on the long-term production of gas. According to Zhou et al. [278], the long-term gas production leads to an elevation in effective stress. Hence, it is imperative to investigate the mechanical properties of sediments containing hydrates across a diverse range of effective confining pressures particularly in the context of CO_2 injection to the hydrate reservoir.

3.4.4. Sediment composition effects

Factors such as particle shape, size distribution, and percentage of fine components can impact the mechanical behaviour of HBS. Since breaking and rearranging of larger particles is more difficult, HBS is more influential in host sediments with more large particles. When the sediments have equal average particle sizes, a broader particle size distribution can potentially increase the HBS strength [279,280], although hydrate coordination number and sand particle surface area can influence this strength. Apart from the pore size distribution, sand particle roundness affects HBS strength. For example, for the same grain size, hydrate saturation, and effective stress, HBS strength increases with sand particle roundness. Under appropriate confining pressure, rounder sand particle shapes show less strain-softening [254]. A higher proportion of fine components may also result in the formation of large clusters of hydrate-cemented sand and fine particles with intergranular strengthening [279]. These hydrate-cemented clusters interact with nearby sand particles to prevent "force chains" from bending during shearing, enhancing microscale dilatation and strength.

The analysis conducted at site 570 of the Deep Sea Drilling Project, located in the Middle America Trench, revealed that sediments containing hydrates exhibited significantly larger particle sizes compared to those lacking hydrates in both the upper and lower strata [281]. Additionally, a substantial proportion of sand and silt was observed in these sediments. Nevertheless, it is worth noting that in the continental slope of the South China Sea, specifically at a depth of 200 m, the sediments predominantly consist of silty sand and clay, with a minimal presence of sand. Based on findings from the Ocean Drilling Program Leg, it was observed that the lower boundary of gas hydrate stability was situated at a depth 40–100 m shallower than the bottom simulating reflection [282]. This discrepancy was attributed to the impact of sediments on the hydrate equilibrium. Furthermore, pore water contains a diverse range of salt ions. The interactions between these ions and water molecules have a significant impact on the hydrates stability [283].

3.4.5. Creep test

Creep, where a geo-strain material increases over time under a specific load, is essential in long-term HBS mechanical behaviour forecasts. HBS creep has four steps: (a) transient creep stage, where elastic or plastic deformation may occur as soon as a load is applied, (b) damping creep stage, where the strain rate is initially high but gradually falls, (c) steady-state creep stage, where the strain rate almost completely stabilizes, and (d) accelerating creep stage, where the material fails quickly as the strain rate index rises. The strain rate is high at transient and damping creep stages but decreases as the creep test advances [234].

Mountjoy et al. demonstrated the potential for creep deformation in methane hydrate-bearing layers [284]. There have been limited reports on creep tests conducted on sediments containing methane hydrates, despite the significance of understanding their creep behaviours in order to forecast the enduring stability of these layers accurately [285]. Parameswaran et al. conducted initial creep tests on frozen sand samples that contained tetrahydrofuran (THF) hydrate at a temperature of 270 K [286]. They successfully obtained creep curves and creep rates for different levels of axial stress. Cameron et al. examined creep characteristics of sands consolidated with THF hydrate under uniaxial compression [287]. They reported that the strength of the hydrate-consolidated sands surpassed that of the sands consolidated with ice. Durham et al. conducted creep tests on high-purity methane hydrate and found that methane hydrate exhibits over 20 times greater strength and resistance to creep compared to ice [288]. The drained triaxial compression creep tests were conducted by Miyazaki et al. on methane hydrate-bearing sand [289]. These tests were then compared to the strain rate dependence of strength observed in constant-strain-rate tests. Their findings indicated that the sand specimen containing methane hydrate exhibited characteristic creep curves and exhibited significant time-dependent behaviour. Miyazaki et al. introduced a nonlinear viscoelastic constitutive equation for sand containing

methane hydrate, which was derived from the analysis of creep phenomena [290]. Li et al., also performed a series of experiments to investigate the creep properties of methane hydrate in the presence of ice [291]. The study focused on examining the influence of deviator stress, confining pressure, and temperature on the creep behaviour of the material.

Based on existing sources [292,293], it has been established that methane hydrate, which is present in Arctic and permafrost regions, has the potential to exist in conjunction with ice. Therefore, it is essential to investigate the creep characteristics of frozen sediments containing methane hydrates (in conjunction with ice) prior to engaging in commercial methane hydrate extraction in Arctic and permafrost areas through different methods including CO_2 injection.

3.4.6. Effect of CO_2 replacement on the mechanical behaviour of HBS

Natural gas hydrates extraction and CO_2 replacement involves disrupting its thermodynamic equilibrium. When considering cost, complexity, and ecological issues, depressurization, thermal stimulation, and CO_2 replacement are the key options. As discussed, CO_2 replacement method stores CO_2 and releases trapped gas from hydrates. It is carried by exerting precise pressure and temperature and adding gas/liquid CO_2 to the HBS [294]. Tri-axial or other geo-mechanical devices have never employed CO_2 replacement due to their operating complexity and low efficiency. CO_2-HBS and CH_4-HBS mechanical characteristics were compared in early testing. In terms of stiffness, strength, stress-strain response, and consolidation properties, CO_2-HBS appears more stable than CH_4-HBS, regardless of whether the temperature is above or below the freezing point (oceanic or permafrost zone) [295]. With the same temperature and pressure, the CO_2 hydrate may have a higher subcooling temperature than the CH_4 hydrate, making it more stable.

3.5. Fluid flow through gas hydrate in the sediment

To investigate economic viability though the CO_2–CH_4 hydrate replacement process, the effect of gas hydrates on permeability must be understood [296]. Shen et al. examined how appropriate confining pressure and triaxial compression affect methane hydrate permeability [297]. Shear band creates a large permeability increase when axial strain exceeds a certain magnitude during shear. Li et al. reported water relative permeability for silts with various methane hydrate saturations [298]. Kneafsey et al. also examined gas permeability of sand and sand-powder mixes in methane hydrate-containing medium [299]. As water content increases, the moist sand's gas permeability drops.

Moreover, as pore space increases, methane hydrate sand deposits' effective permeability often decreases. Zhao et al. injected methane into the sea sediments to test gas permeability [300]. Confining pressure, hydrate saturation, and initial water saturation affect gas permeability. The microscopic process through which hydrate changes flow characteristics were also investigated by Xu et al. [301]. They found five hydrate occurrence methods in sediments with hydrates: particle inclusion, pore filling, throat filling, particle cementation, and bearing.

Zhao et al. developed a Masuda permeability correction model to evaluate dynamic permeability during the depression–reduction process by varying effective stress (0.2–5.0 MPa) and hydrate saturation (36.6–53.1 %) [302]. Deng et al. also formulated the pore compressibility index (PCI) for hydrate sediments [303]. PCI is theoretically linked to permeability. Using logging data, sediments with high permeability showed lower PCI values and higher porosity. Even low hydrate saturation reduces permeability and PCI. Hence, accurate permeability prediction enhances hydrate detection and identification for CO_2–CH_4 hydrate replacement process.

Cui et al. examined methane hydrate dissociation spatially using an L-shaped hydrate simulator [304]. Experiments showed that water migration unevenly emptied sediment pore spaces and affected hydrate breakdown geography. Water seepage and migration trap gas in pores to stop gas production, limiting active fluid migration to a narrow zone [304]. With an increase in flow space, gas flow rate can be kept very low to reduce hydrate formation and resolve the blockage [305,306]. Konno et al. [307] found that hydrate-saturated layers with higher permeability increases the production fluid's gas-to-water ratio. However, water seepage may have transferred sediment and sand from the overlying to the production well, clogging it quickly. Using controlled drawdown rates, Yin et al. examined the cumulative water and gas generation during methane hydrate decomposition [308]. A slow decomposition rate can also regulate the water–gas ratio and increase water production. Gao et al. [309] used multi-stage depressurization to reduce water production and hydrate breakdown, but it reduces gas production efficiency. Nonetheless, several studies on gas hydrate extraction and multiphase flow contain inconsistencies. Therefore, comprehensive studies are required to identify the flow characteristics in the HBS during CO_2 injection.

3.6. Field scale test for hydrate-based CCS

CO_2 storage in the ocean as gas hydrates for CCS is appealing due to the several key factors, such as the vast size of the ocean, the ability of wet sediments to store CO_2 as gas hydrates, large CO_2 storage capacity offered by gas hydrates, the circulating currents of the ocean, and a favourable equilibrium conditions and hydrate stability zones existing in ocean [177]. In the past, some field tests were carried out to extend lab-based gas hydrate studies to real-world applications. Currently, exploratory studies are highly active in the area of natural gas hydrate extraction [310]. A summary of the field scale tests conducted for CCS as gas hydrates in the deep ocean is provided in this section.

Initially, Brewer et al. [311] used the remotely operated vehicle (ROV) to observe methane hydrate formation at a depth of 910 m in Monterey Bay's deep waters. In free seawater, a buoyant mass of transparent CH_4 hydrate was observed to form quickly at the gas-water interface. The pore spaces of a coarse sand matrix were filled with CH_4 hydrates, and the sand column was cemented. Then Brewer et al. [312] later used the same ROV to discharge hydrocarbon gases and liquid CO_2 into natural seawater and marine sediments. Hydrate formation was virtually instantaneous for some gases at 910 m depth and 3.9 °C. Brewer et al. [313] also conducted trials at depths ranging from 349 to 3627 m and at temperatures 8° to 1.6 °C. Hydrate formation occurred promptly from the gaseous state at a depth of 349 m and the seawater-carbon dioxide interface at a depth of 3627 m had a rapid increase due to the formation of significant amounts of hydrates. A reservoir of liquid carbon dioxide expanded more than four times with the formation of hydrate, which would dissolve later.

Brewer et al. [314], later conducted a series of in situ experiments to investigate the formation of a CO_2 hydrate using an ROV in Monterey Bay at a depth of 619 m. The pH measurements made near the hydrate–seawater interface showed a wide range of values, conditional to the method of injection and the surface area of the hydrate formed. Brewer et al. [315] then measured the rise and dissolution rates of freely released CO_2 droplets in the open ocean by releasing liquid CO_2 at 800 m [4.4 °C] and imaging the rising droplet stream. The initial rise rate for 0.9 cm diameter droplets was 10 cm/s at 800 m, and the dissolution rate was 3.0 μmol cm^{-2} s^{-1}. Brewer et al. [316] also developed a carbon-fiber composite accumulator of 56L internal capacity for safely delivering CO_2 in the deep sea. This technique confirmed the rapid re-building of the hydrate skin in which surface cracks are quickly annealed. A small-scale CO_2 sequestration experiment in northern California (684 m depth, ~5 °C, pH ~7.7) was also carried out by Brewer et al. [317]. Their results indicated the rapid CO_2 dissolution, with all CO_2 being depleted in a little more than 2 days. Tsouris et al. [318] injected particulate composites of CO_2 hydrate/liquid CO_2/seawater phases in seawater at depths between 1100 and 1300 m. An ROV tracked the resultant composite particles, and the composite particles' dissolution rate was reported higher than that of pure CO_2 droplets. Rehder

et al. [319], measured the dissolution rates of pure methane and CO_2 hydrates directly on the seafloor within the gas hydrate stability zone. They reported dissolution rates of 4.15 ± 0.5 mmol CO_2/m^2s and 0.37 ± 0.03 mmol CH_4/m^2s. Hester et al. [320], measured the dissolution of natural hydrate cores on the seafloor at Barkley Canyon (850 m depth and 4.17 °C). The flux of gas from the shrinking yellow hydrate core was 0.15 ± 0.01 mmol gas/m^2 s, while the white hydrate dissolved faster at 0.25 ± 0.02 mmol gas/m^2 s. In years later, Brewer et al. [321], carried out a small-scale deep-sea field test to extract CH_4 gas from CH_4 hydrate by injection of a CO_2/N_2 gas mixture. However, they reported a complete and rapid dissociation of the CH_4 hydrate with the release of liquid water and the creation of a mixed gas phase.

It was indicated in earlier field tests that it's not favourable to form CO_2 hydrates on the ocean floor due to susceptible perturbations. This shifted the research interest towards forming and storing CO_2 as gas hydrates in oceanic sediments. However, the long-term stability of these hydrates is the key issue. Recently, Qureshi et al. [164,165,322,323] provided the first-ever experimental evidence of the CO_2 hydrates stability in the sediments at the simulated depth of 1 Km [10 MPa, 4 °C] on the laboratory scale by evaluating their stability in brine/fresh water for 15–30 days using both gas and liquid CO_2. Their experimental results indicate that the formation of CO_2 hydrates is faster with liquid CO_2, and CO_2 hydrates are more stable inside the sediments. Moreover, the use of amino acid [86,324,325] gas hydrate promoters or additives like L-tryptophan [326,327] can significantly enhance the kinetics of CO_2 hydrate formation [328,329]. Hence, many field scale and lab scale studies related to CCS in ocean at depths ranging from 300 to 3600 m have indicated a good potential for CO_2 storage as gas hydrates. However, further large-scale technological demonstrations are still needed to develop a full-scale commercial hydrate-based CCS process.

4. Outlook

Industrial-point-source CCS, Direct Air Capture (DAC), and Bioenergy with Carbon Capture and Storage (BECCS) are today's three primary technological approaches to carbon capture. Of these, Industrial-point-source CCS holds immediate promise for decarbonization, particularly for industries with limited alternative options. By 2030, around 110 million tons per annum (MTPA) of CO_2 is projected to be captured, but to meet the COP26 commitments, this needs to increase to 715 MTPA by 2030 and 4200 MTPA by 2050. However, the adoption and scaling of CCUS face significant challenges [330].

Although there are various approaches for adoption and scaling of CCS, CO_2 hydrate offers the substantial applications for CCS. While this review (part 1 and part 2) shows a significant understanding of CO_2 hydrate and its applications in CCS, there are still various challenges that need to be further investigated. In this closing section, some potential and challenge of hydrate-based CCS are overlooked for future research and development.

Hydrate-based carbon capture (HBCC) presents a promising solution for the efficient CO_2 capture. However, researchers should explore novel materials and operational strategies that not only improve the efficiency of HBCC processes but also reduce energy consumption. It is essential to ensure that this technology is economic and scalable for CCS solutions. Based on estimations, the cost of avoiding 1 tonne of CO_2 through HBCC technology ranges from 20 to 40 US dollars, with an associated energy penalty of 15 %. In comparison, the conventional absorption method currently incurs a cost of 40–100 US dollars per tonne of CO_2, accompanied by an energy penalty of 30 % [331]. Therefore, HBCC exhibits potential competitiveness relative to the conventional absorption approach. HBCC possess a distinct advantage in industrial scales due. Firstly, its utilization of a water-based process sets it apart. Secondly, it exhibits a tolerance towards impurities present in the feed gas. Lastly, there is potential for energy savings through the integration of hydrate formation and dissociation enthalpies. However, the current obstacles to implementation include slow kinetics and a lack of extensive industrial experience [331]. Furthermore, there is limited research pertaining to the assessment of costs associated with HBCC.

The site selection for CCS is another important factor which requires consideration of several economic factors. The injection flow rate, location, pipeline size, and operational conditions all contribute towards the economics of CCS. For example, non-condensable pollutants like N_2, O_2, and Ar, which are often captured with CO_2, may increase storage project costs. These impurities may also reduce site's storage capacity [332]. The costs associated with CO_2 storage rely upon the specific attributes of the geological reservoir. The most cost-effective approach for CO_2 storage involves utilizing onshore depleted oil and gas fields by leveraging pre-existing wells [333]. However, as this review paper shows, there is a potential application for permanently CO_2 storage through CO_2 hydrate formation in geological reservoirs or CO_2/CO_2-rich injection into gas hydrate reservoirs (CO_2–CH_4 exchange process). Furthermore, although the concept of CO_2–CH_4 hydrate replacement process has been proved, further comprehensive studies are required to characterise this concept and flow behaviour in the hydrate bearing sediment.

To enhance the feasibility of CO_2 injection into hydrate reservoirs for the CO_2–CH_4 exchange process, it is essential for the CO_2 capture hub to be in close to the hydrate reservoir. This ensures cost-effectiveness in terms of CO_2 transportation and injection. When dealing with substantial distances between CO_2 capture plants and CO_2 sequestration sites, the expenses associated with CO_2 transportation can surpass the capture process itself [334]. Fig. 10 shows the global map of CCS projects and hydrate reservoirs. This provides an insight into the suitability of the location for CO_2 storage within the gas hydrate reservoir.

It is imperative to acknowledge that most strategies for achieving deep decarbonization are intricately linked to the expansion of the current transport infrastructure and the development of new infrastructure. It can be postulated that the establishment of CO_2 pipeline network would likely entail a comparatively streamlined, cost-effective, and expeditious process in contrast to the development of a hydrogen infrastructure [337]. According to IPCC [338], considerable expertise has been acquired globally in the development and operation of CO_2 pipelines, encompassing both terrestrial and subsea installations. Nevertheless, However, the gas hydrate flow assurance study for the feasibility of CO_2 transportation is required.

CRediT authorship contribution statement

Morteza Aminnaji: Writing – review & editing, Writing – original draft, Validation, Supervision, Software, Methodology, Investigation, Formal analysis, Data curation, Conceptualization. **M Fahed Qureshi:** Writing – review & editing, Writing – original draft, Validation, Investigation, Formal analysis, Data curation. **Hossein Dashti:** Writing – review & editing, Writing – original draft, Validation, Investigation, Formal analysis, Data curation. **Alfred Hase:** Writing – review & editing, Validation, Methodology, Conceptualization. **Abdolali Mosalanejad:** Writing – review & editing, Writing – original draft, Validation, Investigation, Formal analysis, Data curation. **Amir Jahanbakhsh:** Writing – review & editing, Writing – original draft, Validation, Investigation, Formal analysis, Data curation. **Masoud Babaei:** Writing – review & editing, Validation, Methodology, Conceptualization. **Amirpiran Amiri:** Writing – review & editing, Validation, Methodology, Conceptualization. **Mercedes Maroto-Valer:** Writing – review & editing, Validation, Methodology, Conceptualization.

Declaration of competing interest

The authors declare that they have no known competing financial interests or personal relationships that could have appeared to influence the work reported in this paper.

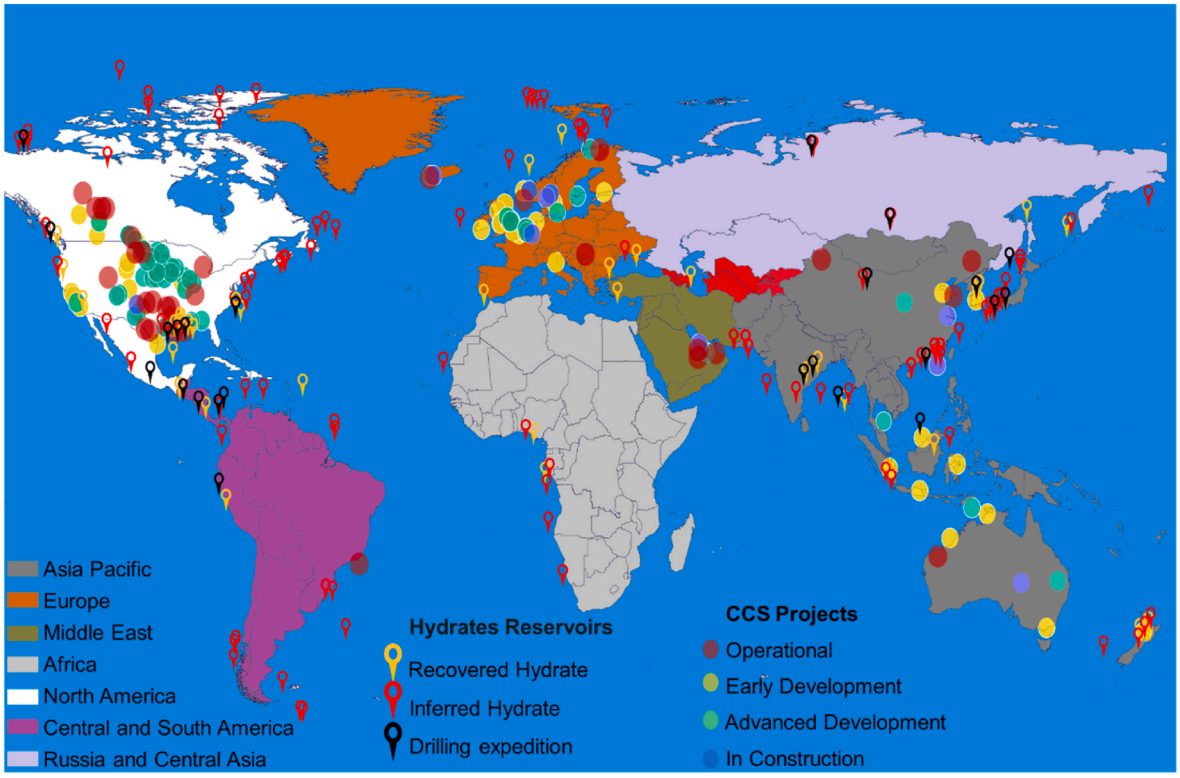

Fig. 10. Global map of CCUS projects and gas hydrate reservoirs. Data for the World Map of CCS Facilities has been extracted from the Global Status of CCS 2022 Report [335]. World Map of gas hydrate has been extracted from United States Geological Survey [336].

Data availability

Data will be made available on request.

Acknowledgements

A. Jahanbakhsh and M. M. Maroto-Valer would like to acknowledge that this work was supported by the UKRI ISCF Industrial Challenge within the UK Industrial Decarbonization Research and Innovation Centre (IDRIC) award number: EP/V027050/1.

References

[1] Kang K, Huh C, Kang S-G, Baek J-H, Noh HJ. Estimation of CO2 pipeline transport cost in South Korea based on the scenarios. Energy Proc 2014;63:2475–80.
[2] Neele F, Koenen M, van Deurzen J, Seebregts A, Groenenberg H, Thielemann T. Large-scale CCS transport and storage networks in north-west and central europe. Energy Proc 2011;4:2740–7.
[3] Lazic T, Oko E, Wang M. Case study on CO2 transport pipeline network design for Humber region in the UK. Proc Inst Mech Eng Part e J Process Mech Eng 2014; 228:210–25.
[4] Xing Y. A conceptual large autonomous subsea freight-glider for liquid CO2 transportation. In: Int. Conf. Offshore mech. Arct. Eng.; 2021, V006T06A052.
[5] Svensson R, Odenberger M, Johnsson F, Strömberg L. Transportation systems for CO2——application to carbon capture and storage. Energy Convers Manag 2004; 45:2343–53.
[6] Michaelides EE. Thermodynamic analysis and power requirements of CO2 capture, transportation, and storage in the ocean. Energy 2021;230:120804.
[7] Skovholt O. CO2 transportation system. Energy Convers Manag 1993;34: 1095–103.
[8] Gao L, Fang M, Li H, Hetland J. Cost analysis of CO2 transportation: case study in China. Energy Proc 2011;4:5974–81.
[9] Smith E, Morris J, Kheshgi H, Teletzke G, Herzog H, Paltsev S. The cost of CO2 transport and storage in global integrated assessment modeling. Int J Greenh Gas Control 2021;109:103367.
[10] Peletiri SP, Rahmanian N, Mujtaba IM. CO2 Pipeline design: a review. Energies 2018;11:2184.
[11] Peletiri PS, Rahmanian N, Mujtaba IM. Effects of impurities on CO 2 pipeline performance. Chem. Eng. Trans. 2017;57:355–60.
[12] Liljemark S, Arvidsson K, Mc Cann MTP, Tummescheit H, Velut S. Dynamic simulation of a carbon dioxide transfer pipeline for analysis of normal operation and failure modes. Energy Proc 2011;4:3040–7.
[13] Zahid U, Lee U, An J, Lim Y, Han C. Economic analysis for the transport and storage of captured carbon dioxide in South Korea. Environ Prog \& Sustain Energy 2014;33:978–92.
[14] Vitali M, Zuliani C, Corvaro F, Marchetti B, Terenzi A, Tallone F. Risks and safety of CO2 transport via pipeline: a review of risk analysis and modeling approaches for accidental releases. Energies 2021;14:4601.
[15] Erdal H. Prediction of pipeline projects construction costs utilizing machine learning techniques. In: Int. Marmara sci. Congr. (Spring 2021); 2021. p. 218.
[16] Arcangeletti G, Aloigi E, Baldoni A, Branduardi L, Castiglioni F, Filippi A, Leporini M, Masi O, Mercuri A, Orselli B. Others, advancing technologies for H2 and CO2 offshore transportation enabling the energy transition: design challenges and opportunities for long distance pipeline systems. In: OMC med energy conf. Exhib.; 2021.
[17] Nazeri M, Haghighi H, Mckay C, Erickson D, Zhai S. Impact of CO2 specifications on design and operation challenges of CO2 transport and storage systems in CCUS. In: SPE offshore eur. Conf. \& Exhib.; 2021.
[18] Arcangeletti G, Scarsciafratte D, Leporini M, Orselli B, Santicchia A, Torselletti E, Aloigi E. The new technological frontiers of CO2 and hydrogen transportation via pipelines. In: Abu dhabi int. Pet. Exhib. \& conf.; 2021.
[19] Handogo R, Mualim A, Sutikno JP, Altway A. Evaluation of CO2 transport design via pipeline in the CCS system with various distance combinations. ECS Trans 2022;107:8593.
[20] Vitali M, Corvaro F, Marchetti B, Terenzi A. Thermodynamic challenges for CO2 pipelines design: a critical review on the effects of impurities, water content, and low temperature. Int J Greenh Gas Control 2022;114:103605.
[21] Suzuki T, Toriumi M, Sakemi T, Masui N, Yano S, Fujita H, Furukawa H. Conceptual design of CO2 transportation system for CCS. Energy Proc. 2013;37: 2989–96.
[22] Qasim A, Khan MS, Lal B, Shariff AM. A perspective on dual purpose gas hydrate and corrosion inhibitors for flow assurance. J Pet Sci Eng 2019;183:106418.
[23] Mokhatab S, Wilkens RJ, Leontaritis KJ. A review of strategies for solving gas-hydrate problems in subsea pipelines. Energy Sources, Part A 2007;29:39–45.
[24] Raja PB, Ismail M, Ghoreishiamiri S, Mirza J, Ismail MC, Kakooei S, Rahim AA. Reviews on corrosion inhibitors: a short view. Chem Eng Commun 2016;203: 1145–56.
[25] Kvamme B, Kuznetsova T, Jensen B, Stensholt S, Bauman J, Sjøblom S, Lervik KN. Consequences of CO2 solubility for hydrate formation from carbon dioxide containing water and other impurities. Phys Chem Chem Phys 2014;16:8623–38.
[26] Kuznetsova T, Jensen B, Kvamme B, Sjøblom S. Water-wetting surfaces as hydrate promoters during transport of carbon dioxide with impurities. Phys Chem Chem Phys 2015;17:12683–97.

[27] E.N. BV, C. Econometrics, others. Assessing the case for EU legislation on the safety of pipelines and the possible impacts of such an initiative. 2013.
[28] Wilday AJ, Moonis M, Wardman MW, Johnson M. Safety in carbon dioxide capture, transport and storage. Buxt. UK Heal. Saf. Lab; 2009.
[29] McCoy ST, Rubin ES. An engineering-economic model of pipeline transport of CO2 with application to carbon capture and storage. Int J Greenh Gas Control 2008;2:219–29.
[30] Uilhoorn FE. Evaluating the risk of hydrate formation in CO2 pipelines under transient operation. Int J Greenh Gas Control 2013;14:177–82.
[31] Wang Z, Zhao Y, Zhang J, Pan S, Yu J, Sun B. Flow assurance during deepwater gas well testing: hydrate blockage prediction and prevention. J Pet Sci Eng 2018; 163:211–6.
[32] Zerpa LE. A practical model to predict gas hydrate formation, dissociation and transportability in oil and gas flowlines. Colorado School of Mines; 2013.
[33] Wang Y, Koh CA, Dapena JA, Zerpa LE. A transient simulation model to predict hydrate formation rate in both oil-and water-dominated systems in pipelines. J Nat Gas Sci Eng 2018;58:126–34.
[34] Shi G, Song S, Shi B, Gong J, Chen D. A new transient model for hydrate slurry flow in oil-dominated flowlines. J Pet Sci Eng 2021;196:108003.
[35] Kwon O, Ryou S, Sung W. Numerical modeling study for the analysis of transient flow characteristics of gas, oil, water, and hydrate flow through a pipeline. Korean J Chem Eng 2001;18:88–93.
[36] Zerpa LE, Sloan ED, Sum AK, Koh CA. Overview of CSMHyK: a transient hydrate formation model. J Pet Sci Eng 2012;98:122–9.
[37] Zare M, Talimi V, Zendehboudi S, Abdi MA. Computational fluid dynamic modeling of methane hydrate formation in a subsea jumper. J Nat Gas Sci Eng 2022;98:104381.
[38] Prah B, Yun R. Heat transfer and flow characteristics of CO2-hydrate mixture in pipeline. Energy Procedia 2017;114:6813–23.
[39] Prah B, Yun R. Heat transfer and pressure drop simulation of CO2-hydrate mixture in tube. Int J Air-Conditioning Refrig 2017;25:1750005.
[40] Prah B, Yun R. Heat transfer and pressure drop of CO2 hydrate mixture in pipeline. Int J Heat Mass Transf 2016;102:341–7.
[41] Lv X, Zuo J, Liu Y, Zhou S-D, Lu D, Shi B, Zhao others H. Experimental study of growth kinetics of CO2 hydrates and multiphase flow properties of slurries in high pressure flow systems. RSC Adv 2019;9:32873–88.
[42] Park H, Yun R. In-Tube convective heat transfer charateristics of Co2-hydrate mixture. In: Int. Heat transf. Conf. Digit. Libr.; 2014.
[43] Oignet J, Hoang HM, Osswald V, Delahaye A, Fournaison L, Haberschill P. Experimental study of convective heat transfer coefficients of CO2 hydrate slurries in a secondary refrigeration loop. Appl Therm Eng 2017;118:630–7.
[44] de Koeijer G, Borch JH, Drescher M, Li H, Wilhelmsen Ø, Jakobsen J. CO2 transport–Depressurization, heat transfer and impurities. Energy Procedia 2011; 4:3008–15.
[45] Yang D, Le LA, Martinez RJ, Currier RP, Spencer DF, Deppe G. Heat transfer during CO2 hydrate formation in a continuous flow reactor. Energy \& Fuels 2008;22:2649–59.
[46] Kvamme B, Kuznetsova T, Kivelæ P-H, Bauman J. Can hydrate form in carbon dioxide from dissolved water? Phys Chem Chem Phys 2013;15:2063–74.
[47] Chapoy A, Burgass R, Tohidi B, Alsiyabi I. Hydrate and phase behavior modeling in CO2-rich pipelines. J Chem \& Eng Data 2015;60:447–53.
[48] Youssef Z, Barreau A, Mougin P, Jose J, Mokbel I. Measurements of hydrate dissociation temperature of methane, ethane, and CO2 in the absence of any aqueous phase and prediction with the cubic plus association equation of state. Ind \& Eng Chem Res 2009;48:4045–50.
[49] Song KY, Kobayashi R. Water content of CO2 in equilibrium with liquid water and/or hydrates. SPE Form Eval 1987;2:500–8.
[50] Burgass R, Chapoy A, Duchet-Suchaux P, Tohidi B. Experimental water content measurements of carbon dioxide in equilibrium with hydrates at (223.15 to 263.15) K and (1.0 to 10.0) MPa. J Chem Thermodyn 2014;69:1–5.
[51] Li H, Jakobsen JP, Stang J. Hydrate formation during CO2 transport: predicting water content in the fluid phase in equilibrium with the CO2-hydrate. Int J Greenh Gas Control 2011;5:549–54.
[52] Adeniyi KI, Deering CE, Grynia E, Marriott RA. Water content and hydrate dissociation conditions for carbon dioxide rich fluid. Int J Greenh Gas Control 2020;101:103139.
[53] Wells JD, Majid AAA, Creek JL, Sloan ED, Borglin SE, Kneafsey TJ, Koh CA. Water content of carbon dioxide at hydrate forming conditions. Fuel 2020;279:118430.
[54] Chapoy A, Nazeri M, Kapateh M, Burgass R, Coquelet C, Tohidi B. Effect of impurities on thermophysical properties and phase behaviour of a CO2-rich system in CCS. Int J Greenh Gas Control 2013;19:92–100. https://doi.org/10.1016/J.IJGGC.2013.08.019.
[55] King MB, Mubarak A, Kim JD, Bott TR. The mutual solubilities of water with supercritical and liquid carbon dioxides. J Supercrit Fluids 1992;5:296–302.
[56] Hou S-X, Maitland GC, Trusler JPM. Measurement and modeling of the phase behavior of the (carbon dioxide+ water) mixture at temperatures from 298.15 K to 448.15 K. J Supercrit Fluids 2013;73:87–96.
[57] Valtz A, Chapoy A, Coquelet C, Paricaud P, Richon D. Vapour–liquid equilibria in the carbon dioxide–water system, measurement and modelling from 278.2 to 318.2 K. Fluid Phase Equilib 2004;226:333–44.
[58] Makiya T, Murakami T, Takeya S, Sum AK, Alavi S, Ohmura R. Synthesis and characterization of clathrate hydrates containing carbon dioxide and ethanol. Phys Chem Chem Phys 2010;12:9927–32.
[59] Semenov AP, Mendgaziev RI, Stoporev AS, Istomin VA, V Sergeeva D, Tulegenov TB, Vinokurov VA. Dimethyl sulfoxide as a novel thermodynamic inhibitor of carbon dioxide hydrate formation. Chem Eng Sci 2022;255:117670.
[60] Cha J-H, Ha C, Kang S-P, Kang JW, Kim K-S. Thermodynamic inhibition of CO2 hydrate in the presence of morpholinium and piperidinium ionic liquids. Fluid Phase Equilib 2016;413:75–9.
[61] Qasim A, Khan MS, Lal B, Shariff AM. Phase equilibrium measurement and modeling approach to quaternary ammonium salts with and without monoethylene glycol for carbon dioxide hydrates. J Mol Liq 2019;282:106–14.
[62] Sa J-H, Lee BR, Park D-H, Han K, Chun HD, Lee K-H. Amino acids as natural inhibitors for hydrate formation in CO2 sequestration. Environ Sci Technol 2011; 45:5885–91.
[63] Mannar N, Bavoh CB, Baharudin AH, Lal B, Mellon NB. Thermophysical properties of aqueous lysine and its inhibition influence on methane and carbon dioxide hydrate phase boundary condition. Fluid Phase Equilib 2017;454:57–63.
[64] Mohammadi AH, Richon D. Phase equilibria of hydrogen sulfide and carbon dioxide simple hydrates in the presence of methanol,(methanol+ NaCl) and (ethylene glycol+ NaCl) aqueous solutions. J Chem Thermodyn 2012;44:26–30.
[65] Najibi H, Kamali Z, Mohammadi AH. Phase equilibria of carbon dioxide clathrate hydrates in the presence of methanol/ethylene glycol+ single salt aqueous solutions: experimental measurement and prediction. Fluid Phase Equilib 2013; 342:71–4.
[66] Dastanian M, Izadpanah AA, Mofarahi M. Phase equilibria of carbon dioxide hydrates in the presence of methanol/ethylene glycol and KCl aqueous solutions. J Chem \& Eng Data 2017;62:1701–7.
[67] Sami NA, Das K, Sangwai JS, Balasubramanian N. Phase equilibria of methane and carbon dioxide clathrate hydrates in the presence of (methanol+ MgCl2) and (ethylene glycol+ MgCl2) aqueous solutions. J Chem Thermodyn 2013;65: 198–203.
[68] Najibi H, Amiri E, Mohammadi AH. Experimental measurement and prediction of dissociation condition for carbon dioxide clathrate hydrates in the presence of methanol/ethylene glycol+ sodium chloride/magnesium chloride aqueous solution. Fluid Phase Equilib 2014;363:70–3.
[69] Dastanian M, Izadpanah AA, Mofarahi M. Experimental measurement of dissociation condition for carbon dioxide hydrates in the presence of methanol/ethylene glycol and CaCl2 aqueous solutions. J Chem \& Eng Data 2018;63: 1675–81.
[70] Maekawa T. Equilibrium conditions for carbon dioxide hydrates in the presence of aqueous solutions of alcohols, glycols, and glycerol. J Chem \& Eng Data 2010; 55:1280–4.
[71] Majumdar A, Mahmoodaghdam E, Bishnoi PR. Equilibrium hydrate formation conditions for hydrogen sulfide, carbon dioxide, and ethane in aqueous solutions of ethylene glycol and sodium chloride. J Chem \& Eng Data 2000;45:20–2.
[72] Breland E, Englezos P. Equilibrium hydrate formation data for carbon dioxide in aqueous glycerol solutions. J Chem \& Eng Data 1996;41:11–3.
[73] Tumba K, Reddy P, Naidoo P, Ramjugernath D, Eslamimanesh A, Mohammadi AH, Richon D. Phase equilibria of methane and carbon dioxide clathrate hydrates in the presence of aqueous solutions of tributylmethylphosphonium methylsulfate ionic liquid. J Chem \& Eng Data 2011;56:3620–9.
[74] Li Z, Zhang Y, Shen Y, Cheng L, Liu B, Yan K, Chen G, Li T. Molecular dynamics simulation to explore the synergistic inhibition effect of kinetic and thermodynamic hydrate inhibitors. Energy 2022;238:121697.
[75] Farhang F, V Nguyen A, Hampton MA. Influence of sodium halides on the kinetics of CO2 hydrate formation. Energy & Fuels 2014;28:1220–9.
[76] Lamorena RB, Lee W. Formation of carbon dioxide hydrate in soil and soil mineral suspensions with electrolytes. Environ Sci \& Technol 2008;42:2753–9.
[77] Liu F-P, Li A-R, Qing S-L, Luo Z-D, Ma Y-L. Formation kinetics, mechanism of CO2 hydrate and its applications. Renew Sustain Energy Rev 2022;159:112221.
[78] Burla SK, Pinnelli SRP, Sain K. Explicating the amino acid effects for methane storage in hydrate form. RSC Adv 2022;12:10178–85. https://doi.org/10.1039/D2RA00531J.
[79] Ke W, Chen D. A short review on natural gas hydrate, kinetic hydrate inhibitors and inhibitor synergists. Chinese J Chem Eng 2019;27:2049–61.
[80] Yagasaki T, Matsumoto M, Tanaka H. Molecular dynamics study of kinetic hydrate inhibitors: the optimal inhibitor size and effect of guest species. J Phys Chem C 2018;123:1806–16.
[81] Li Z, Liao K, Qin H-B, Chen J, Ren L, Li F, Zhang X, Liu B, Chen G. The gas-adsorption mechanism of kinetic hydrate inhibitors. AIChE J 2019;65:e16681.
[82] Aminnaji M, Anderson R, Tohidi B. Anomalous KHI-Induced dissociation of gas hydrates inside the hydrate stability zone: experimental observations & potential mechanisms. J Pet Sci Eng 2019;178:1044–50.
[83] Aminnaji M, Anderson R, Hase A, Tohidi B. Can kinetic hydrate inhibitors inhibit the growth of pre-formed gas hydrates? J Nat Gas Sci Eng 2022;109:104831.
[84] Perrin A, Musa OM, Steed JW. The chemistry of low dosage clathrate hydrate inhibitors. Chem Soc Rev 2013;42:1996–2015.
[85] Zhang Q, Kelland MA, Lu H. Non-amide kinetic hydrate inhibitors: a review. Fuel 2022;315:123179.
[86] Altamash T, Qureshi MF, Aparicio S, Aminnaji M, Tohidi B, Atilhan M. Gas hydrates inhibition via combined biomolecules and synergistic materials at wide process conditions. J Nat Gas Sci Eng 2017;46:873–83.
[87] Kelland MA. A review of kinetic hydrate inhibitors from an environmental perspective. Energy & Fuels 2018;32:12001–12.
[88] Aminnaji M, Anderson R, Jarrahian K, Tohidi B. Natural pectin and commercial luvicap-bio as green kinetic hydrate inhibitors: a comparative evaluation by crystal growth inhibition methods. Energy & Fuels 2022;36:14898–906.
[89] Talaghat MR, Esmaeilzadeh F, Fathikaljahi J. Experimental and theoretical investigation of simple gas hydrate formation with or without presence of kinetic inhibitors in a flow mini-loop apparatus. Fluid Phase Equilib 2009;279:28–40.

[90] Talaghat MR, Bahmani AR. Performance improvement of various kinetic hydrate inhibitors using 2-butoxyethanol for simple gas hydrate formation in a flow mini-loop apparatus. Theor Found Chem Eng 2018;52:438–46.
[91] Shen X-D, Shi L-L, Long Z, Zhou X-B, Liang D-Q. Experimental study on the kinetic effect of N-butyl-N-methylpyrrolidinium bromide on CO2 hydrate. J Mol Liq 2016;223:672–7.
[92] Qureshi MF, Atilhan M, Altamash T, Tariq M, Khraisheh M, Aparicio S, Tohidi B. Gas hydrate prevention and flow assurance by using mixtures of ionic liquids and synergent compounds: combined kinetics and thermodynamic approach. Energy \& Fuels 2016;30:3541–8.
[93] Qureshi MF, Khraisheh M, AlMomani F. Experimentally measured methane hydrate phase equilibria and ionic liquids inhibition performance in Qatar's seawater. Sci Rep 2020;10:19463.
[94] Khan MS, Lal B, Keong LK, Ahmed I. Tetramethyl ammonium chloride as dual functional inhibitor for methane and carbon dioxide hydrates. Fuel 2019;236:251–63.
[95] Roosta H, Dashti A, Mazloumi SH, Varaminian F. Inhibition properties of new amino acids for prevention of hydrate formation in carbon dioxide–water system: experimental and modeling investigations. J Mol Liq 2016;215:656–63.
[96] Sa J-H, Kwak G-H, Lee BR, Park D-H, Han K, Lee K-H. Hydrophobic amino acids as a new class of kinetic inhibitors for gas hydrate formation. Sci Rep 2013;3:1–7.
[97] Sa J-H, Kwak G-H, Han K, Ahn D, Lee K-H. Gas hydrate inhibition by perturbation of liquid water structure. Sci Rep 2015;5:1–9.
[98] Yaqub S, Keong LK. others, Thermodynamic and kinetic effect of biodegradable polymers on carbon dioxide hydrates. J Ind Eng Chem 2019;79:131–45.
[99] Khan MS, Lal B, Shariff AM, Mukhtar H. Ammonium hydroxide ILs as dual-functional gas hydrate inhibitors for binary mixed gas (carbon dioxide and methane) hydrates. J Mol Liq 2019;274:33–44.
[100] Chun LK, Jaafar A. Ionic liquid as low dosage hydrate inhibitor (LDHI) for flow assurance in pipeline. 2012.
[101] Anderson R, Mozaffar H, Tohidi B. Development of a crystal growth inhibition based method for the evaluation of kinetic hydrate inhibitors. In: Proc. 7th int. Conf. Gas hydrates; 2011. p. 17–21.
[102] Mozaffar H, Anderson R, Tohidi B. Reliable and repeatable evaluation of kinetic hydrate inhibitors using a method based on crystal growth inhibition. Energy & Fuels 2016;30:10055–63.
[103] Qureshi MF, Atilhan M, Altamash T, Aparicio S, Aminnaji M, Tohidi B. High-pressure gas hydrate autoclave hydraulic experiments and scale-up modeling on the effect of stirring RPM effect. J Nat Gas Sci Eng 2017;38:50–8.
[104] Aminnaji M. Inhibition and dissociation of gas hydrates using glycols/alcohols and biodegradable kinetic hydrate inhibitors. Heriot-Watt University; 2018. Doctoral dissertation, https://ethos.bl.uk/OrderDetails.do?uin=uk.bl.ethos.777738.
[105] ur Rehman A, Abdulwahab A, Kaur A, Khan MS, Zaini DB, Shariff AM, Lal B. Experimental investigation and modelling of synergistic thermodynamic inhibition of Diethylene Glycol and glycine mixture on CO2 gas hydrates. Chemosphere 2022;308:136181.
[106] Kelland MA, Svartaas TM, Øvsthus J, Tomita T, Mizuta K. Studies on some alkylamide surfactant gas hydrate anti-agglomerants. Chem Eng Sci 2006;61:4290–8.
[107] Chen J, Wang Y-F, Sun C-Y, Li F-G, Ren N, Jia M-L, Yan K-L, Lv Y-N, Liu B, Chen G-J. Evaluation of gas hydrate anti-agglomerant based on laser measurement. Energy & Fuels 2015;29:122–9.
[108] Phan A, Bui T, Acosta E, Krishnamurthy P, Striolo A. Molecular mechanisms responsible for hydrate anti-agglomerant performance. Phys Chem Chem Phys 2016;18:24859–71.
[109] Salmin DC, Estanga D, Koh CA. Review of gas hydrate anti-agglomerant screening techniques. Fuel 2022;319:122862.
[110] Liu Z, Song Y, Liu W, Liu R, Lang C, Li Y. Rheology of methane hydrate slurries formed from water-in-oil emulsion with different surfactants concentrations. Fuel 2020;275:117961. https://doi.org/10.1016/J.FUEL.2020.117961.
[111] Zhang X, Gong J, Yang X, Slupe B, Jin J, Wu N, Sum AK. Functionalized nanoparticles for the dispersion of gas hydrates in slurry flow. ACS Omega 2019;4:13496–508.
[112] Min J, Baek S, Somasundaran P, Lee JW. Anti-adhesive behaviors between solid hydrate and liquid aqueous phase induced by hydrophobic silica nanoparticles. Langmuir 2016;32:9513–22.
[113] Ahuja A, Iqbal A, Iqbal M, Lee JW, Morris JF. Rheology of hydrate-forming emulsions stabilized by surfactant and hydrophobic silica nanoparticles. Energy & Fuels 2018;32:5877–84.
[114] Bbosa B, Ozbayoglu E, Volk M. Experimental investigation of hydrate formation, plugging and flow properties using a high-pressure viscometer with helical impeller. J Pet Explor Prod Technol 2019;9:1089–104.
[115] Lee W, Choi Y, Kim Y, Lim JS, Kang SP. Rheological investigation of methane hydrate formation with biodegradable emulsifiers as anti-agglomerants. J Pet Sci Eng 2019;183:106454. https://doi.org/10.1016/J.PETROL.2019.106454.
[116] Qin Y, Pickering PF, Johns ML, May EF, Aman ZM. A new rheology model for hydrate-in-oil slurries. In: Offshore technol. Conf. Asia; 2018.
[117] Dong S, Firoozabadi A. Hydrate anti-agglomeration and synergy effect in normal octane at varying water cuts and salt concentrations. J Chem Thermodyn 2018;117:214–22.
[118] Zhao X, Fang Q, Qiu Z, Mi S, Wang Z, Geng Q, Zhang Y. Experimental investigation on hydrate anti-agglomerant for oil-free systems in the production pipe of marine natural gas hydrates. Energy 2022;242:122973.
[119] Sun M, Firoozabadi A. New surfactant for hydrate anti-agglomeration in hydrocarbon flowlines and seabed oil capture. J Colloid Interface Sci 2013;402:312–9.
[120] Li M, Dong S, Li B, Liu C. Effects of a naturally derived surfactant on hydrate anti-agglomeration using micromechanical force measurement. J Ind Eng Chem 2018;67:140–7. https://doi.org/10.1016/J.JIEC.2018.06.024.
[121] R. Anderson, M. Aminnaji, B. Tohidi, Effect of gas composition on hydrate growth rate and agglomeration tendency, in: Eur. Conf. Gas hydrate 2022, Angew. Chemie, [n.d].
[122] Aminnaji M, Hase A, Crombie L. Anti-agglomerants: study of hydrate structural, gas composition, hydrate amount, and water cut effect. In: Int. Pet. Technol. Conf. OnePetro; 2023. https://doi.org/10.2523/IPTC-22765-MS. 10.2523/IPTC-22765-MS.
[123] Chua PC, Kelland MA. Study of the gas hydrate anti-agglomerant performance of a series of n-Alkyl-tri (n-butyl) ammonium bromides. Energy \& Fuels 2013;27:1285–92.
[124] Chen Z, Sun J, Wu P, Liu W, Chen C, Lang C, Dai S, Zhou W. Cyclodextrin as a green anti-agglomerant agent in oil–water emulsion containing asphalt. Fuel 2023;335:127041.
[125] Oignet J, Delahaye A, Torré J-P, Dicharry C, Hoang HM, Clain P, Osswald V, Youssef Z, Fournaison L. Rheological study of CO2 hydrate slurry in the presence of Sodium Dodecyl Sulfate in a secondary refrigeration loop. Chem Eng Sci 2017;158:294–303.
[126] Delahaye A, Fournaison L, Jerbi S, Mayoufi N. Rheological properties of CO2 hydrate slurry flow in the presence of additives. Ind \& Eng Chem Res 2011;50:8344–53.
[127] Prah B, Yun R. CO2 hydrate slurry transportation in carbon capture and storage. Appl Therm Eng 2018;128:653–61.
[128] Lv X, Zhang J, Zuo J, Zhao D, Liu Y, Zhou S, Du H, Song S. Study on the formation characteristics of CO2 hydrate and the rheological properties of slurry in a flow system containing surfactants. ACS Omega 2022;7:2444–57.
[129] Prah B, Yun R. Investigations on CO2 hydrate slurry for transportation in carbon capture and storage. J Mech Sci Technol 2019;33:5085–92.
[130] Prah B, Yun R. Pressure drop and flow characteristic of CO2 hydrate slurry formation in the presence of anti-agglomerant in a flow loop facility. J Mech Sci Technol 2021;35:761–70.
[131] Wu Z, Yu Y-S, Zhou S, He C. others, Insights into carbon dioxide hydrate formation, fluid type, and agglomeration in the system with or without tween-80. Fuel 2022;314:123130.
[132] Delahaye A, Fournaison L, Marinhas S, Mart\'\inez MC. Rheological study of CO2 hydrate slurry in a dynamic loop applied to secondary refrigeration. Chem Eng Sci 2008;63:3551–9.
[133] Jerbi S, Delahaye A, Oignet J, Fournaison L, Haberschill P. Rheological properties of CO2 hydrate slurry produced in a stirred tank reactor and a secondary refrigeration loop. Int J Refrig 2013;36:1294–301.
[134] Hu J, Sari O, Homsy P. Investigation of thermo-physical and flow properties of CO2 hydrate slurry. Int J Air-Conditioning Refrig 2011;19:213–29.
[135] Sahu C, Prasad SK, Kumar R, Sangwai JS. High-pressure rheological signatures of CO2 hydrate slurries formed from gaseous and liquid CO2 relevant for refrigeration, pipeline transportation. Carbon Capture, and Geological Sequestration, Sep Purif Technol 2023:123087.
[136] Fu W, Wei W, Wang H, Huang B, Wang Z. Study on the rheology of CO2 hydrate slurry by using the capillary method. J Mar Sci Eng 2022;10:1224.
[137] Aminnaji M, Tohidi B, Burgass R, Atilhan M. Gas hydrate blockage removal using chemical injection in vertical pipes. J Nat Gas Sci Eng 2017;40:17–23.
[138] Aminnaji M, Tohidi B, Burgass R, Atilhan M. Effect of injected chemical density on hydrate blockage removal in vertical pipes: use of MEG/MeOH mixture to remove hydrate blockage. J Nat Gas Sci Eng 2017;45:840–7.
[139] Wei N, Pei J, Li H, Sun W, Xue J. Application of in-situ heat generation plugging removal agents in removing gas hydrate: a numerical study. Fuel 2022;323:124397.
[140] Shi H, Xie W, Yu Y, Zhong Y, Shi Z, others. Application feasibility of composite plugging removal technology in the development of natural gas hydrate. Drill Eng 2022;49:5–15.
[141] Yang J, Feng Y, Zhang B, Tang Y, Jiang Z. A blockage removal technology for natural gas hydrates in the wellbore of an ultra-high pressure sour gas well. Nat Gas Ind B 2021;8:188–94.
[142] Liu Z, Liu Z, Wang J, Yang M, Zhao J, Song Y. Hydrate blockage observation and removal using depressurization in a fully visual flow loop. Fuel 2021;294:120588.
[143] Shi B-H, Ding L, Li W-Q, Lv X-F, Liu Y, Song S-F, Ruan C-Y, Wu H-H, Wang W, Gong J. Investigation on hydrates blockage and restart process mechanisms of CO2 hydrate slurry flow, Asia-Pacific. J Chem Eng 2018;13:e2193.
[144] Lv X, Li W, Shi B, Zhou S. Study on the blockage mechanism of carbon dioxide hydrate slurry and its microscopic particle characteristics. RSC Adv 2018;8:36959–69.
[145] Zatsepina OY, Pooladi-Darvish M. CO2-hydrate formation in depleted gas reservoirs–A methodology for CO2 storage. Energy Procedia 2011;4:3949–56.
[146] Iglauer S. CO2–water–rock wettability: variability, influencing factors, and implications for CO2 geostorage. Acc Chem Res 2017;50:1134–42.
[147] Iglauer S. Optimum storage depths for structural CO2 trapping. Int J Greenh Gas Control 2018;77:82–7.
[148] Takeya S, Muromachi S, Yamamoto Y, Umeda H, Matsuo S. Preservation of CO2 hydrate under different atmospheric conditions. Fluid Phase Equilib 2016;413:137–41. https://doi.org/10.1016/j.fluid.2015.10.036.

[149] Song Y, Wang S, Cheng Z, Huang M, Zhang Y, Zheng J, Jiang L, Liu Y. Dependence of the hydrate-based CO2 storage process on the hydrate reservoir environment in high-efficiency storage methods. Chem Eng J 2021;415:128937.
[150] Chen B, Sun H, Zheng J, Yang M. New insights on water-gas flow and hydrate decomposition behaviors in natural gas hydrates deposits with various saturations. Appl Energy 2020;259:114185.
[151] Chen X, Li S, Zhang P, Chen W, Wu Q, Zhan J, Wang Y. Promoted disappearance of CO2 hydrate self-preservation effect by surfactant SDS. Energies 2021;14:3909.
[152] Liu Y, Zhang L, Yang L, Dong H, Zhao J, Song Y. Behaviors of CO2 hydrate formation in the presence of acid-dissolvable organic matters. Environ Sci \& Technol 2021;55:6206–13.
[153] Kim I, Nole M, Jang S, Ko S, Daigle H, Pope GA, Huh C. Highly porous CO2 hydrate generation aided by silica nanoparticles for potential secure storage of CO2 and desalination. RSC Adv 2017;7:9545–50. https://doi.org/10.1039/C6RA26366F.
[154] Wen Z, Yao Y, Luo W, Lei X. Memory effect of CO2-hydrate formation in porous media. Fuel 2021;299:120922.
[155] Zhang X, Li J, Wang J, Wu Q, Wang Y, Yao Z. Experimental study on formation characteristics of carbon dioxide hydrate in frozen porous media. Int J Green Energy 2021;18:687–96.
[156] Busch A, Amann A, Bertier P, Waschbusch M, Krooss BM. The significance of caprock sealing integrity for CO2 storage. In: SPE int. Conf. CO2 capture, storage, util; 2010. SPE–139588.
[157] Shukla R, Ranjith P, Haque A, Choi X. A review of studies on CO2 sequestration and caprock integrity. Fuel 2010;89:2651–64.
[158] Song Y, Jun S, Na Y, Kim K, Jang Y, Wang J. Geomechanical challenges during geological CO2 storage: a review. Chem Eng J 2023;456:140968.
[159] Koide H, Takahashi M, Tsukamoto H, Shindo Y. Self-trapping mechanisms of carbon dioxide in the aquifer disposal. Energy Convers Manag 1995;36:505–8.
[160] Rochelle CA, Camps AP, Long D, Milodowski A, Bateman K, Gunn D, Jackson P, Lovell MA, Rees J. Can CO2 hydrate assist in the underground storage of carbon dioxide? Geol Soc London, Spec Publ 2009;319:171–83.
[161] Tohidi B, Anderson R, Ben Clennell M, Burgass RW, Biderkab AB. Visual observation of gas-hydrate formation and dissociation in synthetic porous media by means of glass micromodels. Geology 2001;29:867–70.
[162] Tohidi B, Yang J, Salehabadi M, Anderson R, Chapoy A. CO2 hydrates could provide secondary safety factor in subsurface sequestration of CO2. Environ Sci \& Technol 2010;44:1509–14.
[163] Gauteplass J, Almenningen S, Ersland G, Barth T. Hydrate seal formation during laboratory CO2 injection in a cold aquifer. Int J Greenh Gas Control 2018;78:21–6.
[164] Qureshi MF, Khandelwal H, Usadi A, Barckholtz TA, Mhadeshwar AB, Linga P. CO2 hydrate stability in oceanic sediments under brine conditions. Energy 2022;256:124625.
[165] Qureshi MF, Zheng J, Khandelwal H, Venkataraman P, Usadi A, Barckholtz TA, Mhadeshwar AB, Linga P. Laboratory demonstration of the stability of CO2 hydrates in deep-oceanic sediments. Chem Eng J 2022;432:134290.
[166] Gauteplass J, Almenningen S, Ersland G, Barth T, Yang J, Chapoy A. Multiscale investigation of CO2 hydrate self-sealing potential for carbon geo-sequestration. Chem Eng J 2020;381:122646.
[167] Myshakin EM, Saidi WA, Romanov VN, Cygan RT, Jordan KD. Molecular dynamics simulations of carbon dioxide intercalation in hydrated Na-montmorillonite. J Phys Chem C 2013;117:11028–39.
[168] Chen J, Mei S. Gas-saturated carbon dioxide hydrates above sub-seabed carbon sequestration site and the formation of self-sealing cap. Gas Sci Eng 2023;111:204913.
[169] Chen J, Mei S. Formation of self-sealing capability for carbon dioxide sequestration site in shallow sub-seabed sediments by three-phase coexistence. Authorea Prepr. 2022. https://doi.org/10.1002/essoar.10511436.1.
[170] Xu C-G, Li X-S. Research progress on methane production from natural gas hydrates. RSC Adv 2015;5:54672–99.
[171] Boswell R, Collett TS. Current perspectives on gas hydrate resources. Energy Environ Sci 2011;4:1206–15. https://doi.org/10.1039/C0EE00203H.
[172] Kvamme B, Vasilev A. Black Sea hydrate production value and options for clean energy production. RSC Adv 2023;13:20610–45.
[173] Song Y, Zhang L, Lv Q, Yang M, Ling Z, Zhao J. Assessment of gas production from natural gas hydrate using depressurization{,} thermal stimulation and combined methods. RSC Adv 2016;6:47357–67. https://doi.org/10.1039/C6RA05526E.
[174] Park Y, Kim D-Y, Lee J-W, Huh D-G, Park K-P, Lee J, Lee H. Sequestering carbon dioxide into complex structures of naturally occurring gas hydrates. Proc Natl Acad Sci 2006;103:12690–4.
[175] Kvamme B, Vasilev A. Black Sea gas hydrates: safe long terms storage of CO2 with environmentally friendly energy production. Sustain Energy \& Fuels 2023;7:1466–93.
[176] Ors O, Sinayuc C. An experimental study on the CO2-CH4 swap process between gaseous CO2 and CH4 hydrate in porous media. J Pet Sci Eng 2014;119:156–62.
[177] Zheng J, Chong ZR, Qureshi MF, Linga P. Carbon dioxide sequestration via gas hydrates: a potential pathway toward decarbonization. Energy \& Fuels 2020;34:10529–46.
[178] Yuan Q, Sun C-Y, Yang X, Ma P-C, Ma Z-W, Liu B, Ma Q-L, Yang L-Y, Chen G-J. Recovery of methane from hydrate reservoir with gaseous carbon dioxide using a three-dimensional middle-size reactor. Energy 2012;40:47–58.
[179] Stanwix PL, Rathnayake NM, De Obanos FPP, Johns ML, Aman ZM, May EF. Characterising thermally controlled CH4-CO2 hydrate exchange in unconsolidated sediments. Energy \& Environ Sci 2018;11:1828–40.
[180] Lee BR, Koh CA, Sum AK. Quantitative measurement and mechanisms for CH4 production from hydrates with the injection of liquid CO2. Phys Chem Chem Phys 2014;16:14922–7.
[181] Ersland G, Husebø J, Graue A, Kvamme B. Transport and storage of CO2 in natural gas hydrate reservoirs. Energy Procedia 2009;1:3477–84.
[182] Tegze G, Gránásy L, Kvamme B. Phase field modeling of CH4 hydrate conversion into CO2 hydrate in the presence of liquid CO2. Phys Chem Chem Phys 2007;9:3104–11.
[183] Wang X, Sang DK, Chen J, Mi J. Theoretical insights into nucleation of CO2 and CH4 hydrates for CO2 capture and storage. Phys Chem Chem Phys 2014;16:26929–37.
[184] Ota M, Morohashi K, Abe Y, Watanabe M, Smith Jr RL, Inomata H. Replacement of CH4 in the hydrate by use of liquid CO2. Energy Convers Manag 2005;46:1680–91.
[185] Kvamme B, Graue A, Buanes T, Kuznetsova T, Ersland G. Storage of CO2 in natural gas hydrate reservoirs and the effect of hydrate as an extra sealing in cold aquifers. Int J Greenh Gas Control 2007;1:236–46.
[186] Kvamme B, Graue A, Aspenes E, Kuznetsova T, Gránásy L, Tóth G, Pusztai T, Tegze G. Kinetics of solid hydrate formation by carbon dioxide: phase field theory of hydrate nucleation and magnetic resonance imaging. Phys Chem Chem Phys 2004;6:2327–34.
[187] Koh D-Y, Kang H, Lee J-W, Park Y, Kim S-J, Lee J, Lee JY, Lee H. Energy-efficient natural gas hydrate production using gas exchange. Appl Energy 2016;162:114–30.
[188] Bai D, Zhang X, Chen G, Wang W. Replacement mechanism of methane hydrate with carbon dioxide from microsecond molecular dynamics simulations. Energy \& Environ Sci 2012;5:7033–41.
[189] Pandey JS, Karantonidis C, Karcz AP, von Solms N. Enhanced CH4-CO2 hydrate swapping in the presence of low dosage methanol. Energies 2020;13:5238.
[190] Gambelli AM, Castellani B, Nicolini A, Rossi F. Water salinity as potential aid for improving the carbon dioxide replacement process' effectiveness in natural gas hydrate reservoirs. Processes 2020;8:1298.
[191] Vidal-Vidal Á, Pérez-Rodríguez M, Piñeiro MM. Direct transition mechanism for molecular diffusion in gas hydrates. RSC Adv 2016;6:1966–72. https://doi.org/10.1039/C5RA17867C.
[192] Sujith KS, Ramachandran CN. Carbon dioxide induced bubble formation in a CH4-CO2-H2O ternary system: a molecular dynamics simulation study. Phys Chem Chem Phys 2016;18:3746–54.
[193] Yeon S-H, Seol J, Koh D-Y, Seo Y, Park K-P, Huh D-G, Lee J, Lee H. Abnormal methane occupancy of natural gas hydrates in deep sea floor sediments. Energy \& Environ Sci 2011;4:421–4.
[194] Ueno H, Akiba H, Akatsu S, Ohmura R. Crystal growth of clathrate hydrates formed with methane+ carbon dioxide mixed gas at the gas/liquid interface and in liquid water. New J Chem 2015;39:8254–62.
[195] Mu L, von Solms N. Methane production and carbon capture by hydrate swapping. Energy \& Fuels 2017;31:3338–47.
[196] Wang T, Zhang L, Sun L, Zhou R, Dong B, Yang L, Li Y, Zhao J, Song Y. Methane recovery and carbon dioxide storage from gas hydrates in fine marine sediments by using CH4/CO2 replacement. Chem Eng J 2021;425:131562.
[197] Wei W-N, Li B, Gan Q, Li Y-L. Research progress of natural gas hydrate exploitation with CO2 replacement: a review. Fuel 2022;312:122873.
[198] Xie Y, Zhu Y-J, Zheng T, Yuan Q, Sun C-Y, Yang L-Y, Chen G-J. Replacement in CH4-CO2 hydrate below freezing point based on abnormal self-preservation differences of CH4 hydrate. Chem Eng J 2021;403:126283.
[199] Ohgaki K, Takano K, Sangawa H, Matsubara T, Nakano S. Methane exploitation by carbon dioxide from gas hydrates—phase equilibria for CO2-CH4 mixed hydrate system. J Chem Eng Japan 1996;29:478–83.
[200] Liu Y, Wang P, Yang M, Zhao Y, Zhao J, Song Y. CO2 sequestration in depleted methane hydrate sandy reservoirs. J Nat Gas Sci Eng 2018;49:428–34.
[201] Lee Y, Choi W, Shin K, Seo Y. CH4-CO2 replacement occurring in sII natural gas hydrates for CH4 recovery and CO2 sequestration. Energy Convers Manag 2017;150:356–64.
[202] Merkel FS, Schultz HJ. Methane extraction from natural gas hydrate reservoirs with simultaneous storage of carbon dioxide. Chemie Ing Tech 2015;87:475–83.
[203] Hyodo M, Li Y, Yoneda J, Nakata Y, Yoshimoto N, Kajiyama S, Nishimura A, Song Y. A comparative analysis of the mechanical behavior of carbon dioxide and methane hydrate-bearing sediments. Am Mineral 2014;99:178–83.
[204] Peter E, Messah M, Chau J. Gas recovery through the injection of carbon dioxide or concentrated flue gas in a natural gas hydrate reservoir. In: Offshore technol. Conf. Asia; 2018.
[205] Almenningen S, Flatlandsmo J, Kovscek AR, Ersland G, Fernø MA. Determination of pore-scale hydrate phase equilibria in sediments using lab-on-a-chip technology. Lab Chip 2017;17:4070–6. https://doi.org/10.1039/C7LC00719A.
[206] Boswell R, Schoderbek D, Collett TS, Ohtsuki S, White M, Anderson BJ. The Ignik Sikumi field experiment, Alaska North Slope: design, operations, and implications for CO2–CH4 exchange in gas hydrate reservoirs. Energy \& Fuels 2017;31:140–53.
[207] Zhou X, Liang D, Liang S, Yi L, Lin F. Recovering CH4 from natural gas hydrates with the injection of CO2–N2 gas mixtures. Energy \& Fuels 2015;29:1099–106.
[208] Pandey JS, Khan S, Karcz AP, von Solms N. Chemically modified hydrate swapping and hydrate stability during multistage CO2-N2 injection schemes. Fuel 2021;299:120711.
[209] Kvamme B. Feasibility of simultaneous CO2 storage and CH4 production from natural gas hydrate using mixtures of CO2 and N2. Can J Chem 2015;93:897–905.

[210] Sun Y-F, Zhong J-R, Li R, Zhu T, Cao X-Y, Chen G-J, Wang X-H, Yang L-Y, Sun C-Y. Natural gas hydrate exploitation by CO2/H2 continuous Injection-Production mode. Appl Energy 2018;226:10–21.
[211] Sun Y-F, Wang Y-F, Zhong J-R, Li W-Z, Li R, Cao B-J, Kan J-Y, Sun C-Y, Chen G-J. Gas hydrate exploitation using CO2/H2 mixture gas by semi-continuous injection-production mode. Appl Energy 2019;240:215–25.
[212] Kaur SP, Sujith KS, Ramachandran CN. Formation of a nanobubble and its effect on the structural ordering of water in a CH4-N2-CO2-H2O mixture. Phys Chem Chem Phys 2018;20:9157–66.
[213] Saeidi N, Dunn-Rankin D, Kvamme B, Chien Y-C. Experimental studies on combined production of CH4 and safe long-term storage of CO2 in the form of solid hydrate in sediment. Phys Chem Chem Phys 2021;23:23313–24.
[214] Kvenvolden KA. Methane hydrates and global climate. Global Biogeochem Cycles 1988;2:221–9.
[215] Hester KC, Brewer PG. Clathrate hydrates in nature. Ann Rev Mar Sci 2009;1:303–27.
[216] Miller SL, Smythe WD. Carbon dioxide clathrate in the Martian ice cap. Science (80-) 1970;170:531–3.
[217] Milton DJ. Carbon dioxide hydrate and floods on Mars. Science (80-) 1974;183:654–6.
[218] Cui J-L, Sun Z-F, Kan J-Y, Jia S, Sun C-Y, Chen G-J, Wang X-H, Yuan Q, Li N. Study on the factors affecting the sealing performance and mechanical stability of CO2 hydrate cap during gas production from methane hydrate. J Nat Gas Sci Eng 2021;93:104050.
[219] Sun Z-F, Li N, Jia S, Cui J-L, Yuan Q, Sun C-Y, Chen G-J. A novel method to enhance methane hydrate exploitation efficiency via forming impermeable overlying CO2 hydrate cap. Appl Energy 2019;240:842–50.
[220] Boswell R. Is gas hydrate energy within reach? Science (80-) 2009;325:957–8.
[221] Brown HE, Holbrook WS, Hornbach MJ, Nealon J. Slide structure and role of gas hydrate at the northern boundary of the Storegga Slide, offshore Norway. Mar Geol 2006;229:179–86.
[222] Dawe RA, Thomas S. A large potential methane source—natural gas hydrates. Energy Sources, Part A 2007;29:217–29.
[223] Ning F, Yu Y, Kjelstrup S, Vlugt TJH, Glavatskiy K. Mechanical properties of clathrate hydrates: status and perspectives. Energy \& Environ Sci 2012;5:6779–95.
[224] Rutqvist J, Moridis GJ, Grover T, Collett T. Geomechanical response of permafrost-associated hydrate deposits to depressurization-induced gas production. J Pet Sci Eng 2009;67:1–12.
[225] Wu P, Li Y, Liu W, Liu Y, Wang D, Song Y. Microstructure evolution of hydrate-bearing sands during thermal dissociation and ensued impacts on the mechanical and seepage characteristics. J Geophys Res Solid Earth 2020;125:e2019JB019103.
[226] Pinkert S, Grozic JLH. Failure mechanisms in cemented hydrate-bearing sands. J Chem \& Eng Data 2015;60:376–82.
[227] Yoneda J, Jin Y, Katagiri J, Tenma N. Strengthening mechanism of cemented hydrate-bearing sand at microscales. Geophys Res Lett 2016;43:7442–50.
[228] Hyodo M, Yoneda J, Yoshimoto N, Nakata Y. Mechanical and dissociation properties of methane hydrate-bearing sand in deep seabed. Soils Found 2013;53:299–314.
[229] Hyodo M, Li Y, Yoneda J, Nakata Y, Yoshimoto N, Nishimura A, Song Y. Mechanical behavior of gas-saturated methane hydrate-bearing sediments. J Geophys Res Solid Earth 2013;118:5185–94.
[230] Iwai H, Konishi Y, Saimyou K, Kimoto S, Oka F. Rate effect on the stress-strain relations of synthetic carbon dioxide hydrate-bearing sand and dissociation tests by thermal stimulation. Soils Found 2018;58:1113–32.
[231] Miyazaki K, Masui A, Sakamoto Y, Aoki K, Tenma N, Yamaguchi T. Triaxial compressive properties of artificial methane-hydrate-bearing sediment. J Geophys Res Solid Earth 2011;116.
[232] Pinkert S, Grozic JLH. Experimental verification of a prediction model for hydrate-bearing sand. J Geophys Res Solid Earth 2016;121:4147–55.
[233] Li Y, Song Y, Yu F, Liu W, Zhao J. Experimental study on mechanical properties of gas hydrate-bearing sediments using kaolin clay. China Ocean Eng 2011;25:113.
[234] Li Y, Wu P, Sun X, Liu W, Song Y, Zhao J. Creep behaviors of methane hydrate-bearing frozen sediments. Energies 2019;12:251.
[235] Jin Y, Konno Y, Nagao J. Pressurized subsampling system for pressured gas-hydrate-bearing sediment: microscale imaging using X-ray computed tomography. Rev Sci Instrum 2014;85.
[236] Takeya S, Yoneyama A, Ueda K, Hyodo K, Takeda T, Mimachi H, Takahashi M, Iwasaki T, Sano K, Yamawaki H. others, Nondestructive imaging of anomalously preserved methane clathrate hydrate by phase contrast X-ray imaging. J Phys Chem C 2011;115:16193–9.
[237] Mitchell JK, Soga K. others, Fundamentals of soil behavior. New York: John Wiley \& Sons; 2005.
[238] Wang L, Sun X, Shen S, Wu P, Liu T, Liu W, Zhao J, Li Y. Undrained triaxial tests on water-saturated methane hydrate–bearing clayey-silty sediments of the South China Sea. Can Geotech J 2021;58:351–66.
[239] Kajiyama S, Hyodo M, Nakata Y, Yoshimoto N, Wu Y, Kato A. Shear behaviour of methane hydrate bearing sand with various particle characteristics and fines. Soils Found 2017;57:176–93.
[240] Jiang M, Peng D, Ooi JY. DEM investigation of mechanical behavior and strain localization of methane hydrate bearing sediments with different temperatures and water pressures. Eng Geol 2017;223:92–109.
[241] Shen S, Li Y, Sun X, Wang L, Song Y. Mechanical properties of methane hydrate-bearing sandy sediments under various temperatures and pore pressures. J Pet Sci Eng 2022;208:109474.
[242] Jiang M, Sun R, Arroyo M, Du W. Salinity effects on the mechanical behaviour of methane hydrate bearing sediments: a DEM investigation. Comput Geotech 2021;133:104067.
[243] Chen B, Liu Z, Sun H, Zhao G, Sun X, Yang M. The synthetic effect of traditional-thermodynamic-factors (temperature, salinity, pressure) and fluid flow on natural gas hydrate recovery behaviors. Energy 2021;233:121147.
[244] Higo Y, Oka F, Sato T, Matsushima Y, Kimoto S. Investigation of localized deformation in partially saturated sand under triaxial compression using microfocus X-ray CT with digital image correlation. Soils Found 2013;53:181–98.
[245] Wu P, Li Y, Liu W, Sun X, Kong X, Song Y. Cementation failure behavior of consolidated gas hydrate-bearing sand. J Geophys Res Solid Earth 2020;125:e2019JB018623.
[246] Ghiassian H, Grozic JLH. Strength behavior of methane hydrate bearing sand in undrained triaxial testing. Mar Pet Geol 2013;43:310–9.
[247] Grozic JLH, Ghiassian H. Undrained shear strength of methane hydrate-bearing sand; preliminary laboratory results. In: Proc., 63rd can. Geotech. Conf; 2010. p. 459–66.
[248] Li F-G, Sun C-Y, Zhang Q, Liu X-X, Guo X-Q, Chen G-J. Laboratory measurements of the effects of methane/tetrahydrofuran concentration and grain size on the P-wave velocity of hydrate-bearing sand. Energy \& Fuels 2011;25:2076–82.
[249] Yun TS, Francisca FM, Santamarina JC, Ruppel C. Compressional and shear wave velocities in uncemented sediment containing gas hydrate. Geophys Res Lett 2005;32.
[250] Maslin M, Owen M, Betts R, Day S, Dunkley Jones T, Ridgwell A. Gas hydrates: past and future geohazard? Philos Trans R Soc A Math Phys Eng Sci 2010;368:2369–93.
[251] Iwai H, Konishi Y, Kimoto S. Undrained triaxial compression tests on artificial CO2-hydrate-bearing sand specimens. Energy Procedia 2017;114:3175–84.
[252] Sun ZM, Zhang J, Liu CL, Zhao SJ, Ye YG. Experimental study on the in situ mechanical properties of methane hydrate-bearing sediments. Appl Mech Mater 2013;275:326–31.
[253] Wu P, Li Y, Sun X, Liu W, Song Y. Mechanical characteristics of hydrate-bearing sediment: a review. Energy \& Fuels 2020;35:1041–57.
[254] Kajiyama S, Wu Y, Hyodo M, Nakata Y, Nakashima K, Yoshimoto N. Experimental investigation on the mechanical properties of methane hydrate-bearing sand formed with rounded particles. J Nat Gas Sci Eng 2017;45:96–107.
[255] Miyazaki K, Oikawa Y, Haneda H, Yamaguchi T. Triaxial compressive property of artificial CO2-hydrate sand. Int J Offshore Polar Eng 2016;26:315–20.
[256] Mahabadi N, Zheng X, Jang J. The effect of hydrate saturation on water retention curves in hydrate-bearing sediments. Geophys Res Lett 2016;43:4279–87.
[257] Mahabadi N, Jang J. Relative water and gas permeability for gas production from hydrate-bearing sediments. Geochemistry, Geophys Geosystems 2014;15:2346–53.
[258] Kleinberg RL, Flaum C, Griffin DD, Brewer PG, Malby GE, Peltzer ET, Yesinowski JP. Deep sea NMR: methane hydrate growth habit in porous media and its relationship to hydraulic permeability, deposit accumulation, and submarine slope stability. J Geophys Res Solid Earth 2003;108.
[259] Liang H, Song Y, Chen Y, Liu Y. The measurement of permeability of porous media with methane hydrate. Pet Sci Technol 2011;29:79–87.
[260] Kang DH, Yun TS, Kim KY, Jang J. Effect of hydrate nucleation mechanisms and capillarity on permeability reduction in granular media. Geophys Res Lett 2016;43:9018–25.
[261] Jakobsen M, Hudson JA, Minshull TA, Singh SC. Elastic properties of hydrate-bearing sediments using effective medium theory. J Geophys Res Solid Earth 2000;105:561–77.
[262] Lee MW, Collett TS. Elastic properties of gas hydrate-bearing sediments. Geophysics 2001;66:763–71.
[263] Santamarina JC, Dai S, Terzariol M, Jang J, Waite WF, Winters WJ, Nagao J, Yoneda J, Konno Y, Fujii T. others, Hydro-bio-geomechanical properties of hydrate-bearing sediments from Nankai Trough. Mar Pet Geol 2015;66:434–50.
[264] Ta XH, Yun TS, Muhunthan B, Kwon T-H. Observations of pore-scale growth patterns of carbon dioxide hydrate using X-ray computed microtomography. Geochemistry, Geophys Geosystems 2015;16:912–24.
[265] Xiong L, Li X, Wang Y, Xu C. Experimental study on methane hydrate dissociation by depressurization in porous sediments. Energies 2012;5:518–30.
[266] Winters WJ, Waite WF, Mason DH, Gilbert LY, Pecher IA. Methane gas hydrate effect on sediment acoustic and strength properties. J Pet Sci Eng 2007;56:127–35.
[267] Kim A-R, Kim J-T, Cho G-C, Lee JY. Methane production from marine gas hydrate deposits in Korea: thermal-hydraulic-mechanical simulation on production wellbore stability. J Geophys Res Solid Earth 2018;123:9555–69.
[268] Yoneda J, Masui A, Konno Y, Jin Y, Kida M, Katagiri J, Nagao J, Tenma N. Pressure-core-based reservoir characterization for geomechanics: insights from gas hydrate drilling during 2012–2013 at the eastern Nankai Trough. Mar Pet Geol 2017;86:1–16.
[269] Boswell R, Myshakin E, Moridis G, Konno Y, Collett TS, Reagan M, Ajayi T, Seol Y. India National Gas Hydrate Program Expedition 02 summary of scientific results: numerical simulation of reservoir response to depressurization. Mar Pet Geol 2019;108:154–66.
[270] Hyodo M, Li Y, Yoneda J, Nakata Y, Yoshimoto N, Nishimura A. Effects of dissociation on the shear strength and deformation behavior of methane hydrate-bearing sediments. Mar Pet Geol 2014;51:52–62.
[271] Choi J-H, Lin J-S, Dai S, Lei L, Seol Y. Triaxial compression of hydrate-bearing sediments undergoing hydrate dissociation by depressurization. Geomech Energy Environ 2020;23:100187.

[272] Tabatabaie SH, Pooladi-Darvish M. Analytical solution for gas production from hydrate reservoirs underlain with free gas. J Nat Gas Sci Eng 2009;1:46–57.
[273] Ito T, Komatsu Y, Fujii T, Suzuki K, Egawa K, Nakatsuka Y, Konno Y, Yoneda J, Jin Y, Kida M. others, Lithological features of hydrate-bearing sediments and their relationship with gas hydrate saturation in the eastern Nankai Trough, Japan. Mar Pet Geol 2015;66:368–78.
[274] Collett TS, Boswell R, Cochran JR, Kumar P, Lall M, Mazumdar A, Ramana MV, Ramprasad T, Riedel M, Sain K. Others, geologic implications of gas hydrates in the offshore of India: results of the national gas hydrate Program expedition 01. Mar Pet Geol 2014;58:3–28.
[275] Uchida S, Klar A, Yamamoto K. Sand production model in gas hydrate-bearing sediments. Int J Rock Mech Min Sci 2016;86:303–16.
[276] Cohen E, Klar A, Yamamoto K. Micromechanical investigation of stress relaxation in gas hydrate-bearing sediments due to sand production. Energies 2019;12:2131.
[277] Lei L, Seol Y. Pore-scale investigation of methane hydrate-bearing sediments under triaxial condition. Geophys Res Lett 2020;47:e2019GL086448.
[278] Zhou M, Soga K, Yamamoto K, Huang H. Geomechanical responses during depressurization of hydrate-bearing sediment formation over a long methane gas production period. Geomech Energy Environ 2020;23:100111.
[279] Madhusudhan BN, Clayton CRI, Priest JA. The effects of hydrate on the strength and stiffness of some sands. J Geophys Res Solid Earth 2019;124:65–75.
[280] Luo T, Li Y, Sun X, Shen S, Wu P. Effect of sediment particle size on the mechanical properties of CH4 hydrate-bearing sediments. J Pet Sci Eng 2018;171:302–14.
[281] Shicai S, Linlin G, Zhendong Y, Haifei L, Yanmin L. Thermophysical properties of natural gas hydrates: a reviews. Nat Gas Ind B 2022. https://doi.org/10.1016/J.NGIB.2022.04.003.
[282] Paull CK, Borowski WS, Rodriguez NM. THE ODP LEG 164 SHIPBOARD SCIENTIFIC PARTY, gas hydrates relev. To world margin stab. Clim Chang 1998;137:153.
[283] Mohammadi AH, Afzal W, Richon D. Gas hydrates of methane, ethane, propane, and carbon dioxide in the presence of single NaCl, KCl, and CaCl2 aqueous solutions: experimental measurements and predictions of dissociation conditions. J Chem Thermodyn 2008;40:1693–7.
[284] Mountjoy J, Pecher I, Henrys S, Barnes P, Plaza-Faverola A. Creeping deformation mechanisms for mixed hydrate-sediment submarine landslides. In: EGU gen. Assem. . Conf. Abstr.; 2013. EGU2013–3489.
[285] Miyazaki K, Yamaguchi T, Sakamoto Y, Aoki K. Time-dependent behaviors of methane-hydrate bearing sediments in triaxial compression test. Int J JCRM 2011;7:43–8.
[286] Parameswaran VR, Paradis M, Handa YP. Strength of frozen sand containing tetrahydrofuran hydrate. Can Geotech J 1989;26:479–83.
[287] Cameron I, Handa YP, Baker THW. Compressive strength and creep behavior of hydrate-consolidated sand. Can Geotech J 1990;27:255–8.
[288] Durham WB, Kirby SH, Stern LA, Zhang W. The strength and rheology of methane clathrate hydrate. J Geophys Res Solid Earth 2003;108.
[289] Miyazaki K, Yamaguchi T, Sakamoto Y, Haneda H, Ogata Y, Aoki K, Okubo S. Creep of sediment containing synthetic methane hydrate. J MMIJ 2009;125:156–64.
[290] Miyazaki K, Endo Y, Tenma N, Yamaguchi T. Constitutive equation for triaxial compression creep of artificial methane-hydrate-bearing sand. J MMIJ 2015;131:47–55.
[291] Li Y, Liu W, Song Y, Yang M, Zhao J. Creep behaviors of methane hydrate coexisting with ice. J Nat Gas Sci Eng 2016;33:347–54.
[292] Dallimore SR, Collett TS. Gas hydrates associated with deep permafrost in the Mackenzie delta, NWT, Canada: regional overview. In: Seventh int. Conf. Proc. Permafrost. Univ. Laval. Cent. d'études Nord.; 1998.
[293] Qingbai W, Guanli J, Peng Z. Assessing the permafrost temperature and thickness conditions favorable for the occurrence of gas hydrate in the Qinghai–Tibet Plateau. Energy Convers Manag 2010;51:783–7.
[294] Zhang L, Yang L, Wang J, Zhao J, Dong H, Yang M, Liu Y, Song Y. Enhanced CH4 recovery and CO2 storage via thermal stimulation in the CH4/CO2 replacement of methane hydrate. Chem Eng J 2017;308:40–9.
[295] Luo T, Li Y, Madhusudhan BN, Zhao J, Song Y. Comparative analysis of the consolidation and shear behaviors of CH4 and CO2 hydrate-bearing silty sediments. J Nat Gas Sci Eng 2020;75:103157.
[296] Yang L, Liu Y, Zhang H, Xiao B, Guo X, Wei R, Xu L, Sun L, Yu B, Leng S. others, the status of exploitation techniques of natural gas hydrate. Chinese J Chem Eng 2019;27:2133–47.
[297] Shen S, Li Y, Sun X, Wang L, Song Y. Experimental study on the permeability of methane hydrate-bearing sediments during triaxial loading. J Nat Gas Sci Eng 2020;82:103510.
[298] Li G, Xu Z-L, Li X-S, Shen P-F, Lv Q-N. Permeability investigation and hydrate migration of hydrate–bearing silty sands and silt. J Nat Gas Sci Eng 2021;89:103891.
[299] Kneafsey TJ, Seol Y, Gupta A, Tomutsa L. Permeability of laboratory-formed methane-hydrate-bearing sand: measurements and observations using X-ray computed tomography. Spe J 2011;16:78–94.
[300] Zhao J, Zheng J, Li F, Yang M. Gas permeability characteristics of marine sediments with and without methane hydrates in a core holder. J Nat Gas Sci Eng 2020;76:103215.
[301] Xu J, Bu Z, Li H, Li S, Sun B. Pore-scale flow simulation on the permeability in hydrate-bearing sediments. Fuel 2022;312:122681.
[302] Zhao J, Zheng J, Kang T, Chen B, Yang M, Song Y. Dynamic permeability and gas production characteristics of methane hydrate-bearing marine muddy cores: experimental and modeling study. Fuel 2021;306:121630.
[303] Deng W, Liang J, Kuang Z, Zhang W, He Y, Meng M, Zhong T. Permeability prediction for unconsolidated hydrate reservoirs with pore compressibility and porosity inversion in the northern South China Sea. J Nat Gas Sci Eng 2021;95:104161.
[304] Cui J, Li K, Cheng L, Li Q, Sun Z, Xiao P, Li X, Chen G, Sun C. Experimental investigation on the spatial differences of hydrate dissociation by depressurization in water-saturated methane hydrate reservoirs. Fuel 2021;292:120277.
[305] Wang Y-F, Wang L-B, Li Y, Gu J-X, Sun C-Y, Chen G-J, Wang X-H, Yuan Q, Li N. Effect of temperature on gas production from hydrate-bearing sediments by using a large 196-L reactor. Fuel 2020;275:117963.
[306] Li N, Sun Z-F, Sun C-Y, Li P, Chen G-J, Ma Q-L, Liu B. Simulating natural hydrate formation and accumulation in sediments from dissolved methane using a large three-dimensional simulator. Fuel 2018;216:612–20.
[307] Konno Y, Fujii T, Sato A, Akamine K, Naiki M, Masuda Y, Yamamoto K, Nagao J. Key findings of the world's first offshore methane hydrate production test off the coast of Japan: toward future commercial production. Energy \& Fuels 2017;31:2607–16.
[308] Yin Z, Wan Q-C, Gao Q, Linga P. Effect of pressure drawdown rate on the fluid production behaviour from methane hydrate-bearing sediments. Appl Energy 2020;271:115195.
[309] Gao Q, Yin Z, Zhao J, Yang D, Linga P. Tuning the fluid production behaviour of hydrate-bearing sediments by multi-stage depressurization. Chem Eng J 2021;406:127174.
[310] Liu J-W, Li X-S. Recent advances on natural gas hydrate exploration and development in the South China Sea. Energy \& Fuels 2021;35:7528–52.
[311] Brewer PG, Orr Jr FM, Friederich G, Kvenvolden KA, Orange DL, McFarlane J, Kirkwood W. Deep-ocean field test of methane hydrate formation from a remotely operated vehicle. Geology 1997;25:407–10.
[312] Brewer PG, Orr FM, Friederich G, Kvenvolden KA, Orange DL. Gas hydrate formation in the deep sea: in situ experiments with controlled release of methane, natural gas, and carbon dioxide. Energy \& Fuels 1998;12:183–8.
[313] Brewer PG, Friederich G, Peltzer ET, Orr Jr FM. Direct experiments on the ocean disposal of fossil fuel CO2. Science (80-) 1999;284:943–5.
[314] Brewer PG, Peltzer ET, Friederich G, Aya I, Yamane K. Experiments on the ocean sequestration of fossil fuel CO2: pH measurements and hydrate formation. Mar Chem 2000;72:83–93.
[315] Brewer PG, Peltzer ET, Friederich G, Rehder G. Experimental determination of the fate of rising CO2 droplets in seawater. Environ Sci \& Technol 2002;36:5441–6.
[316] Brewer PG, Peltzer ET, Rehder G, Dunk R. Advances in deep-ocean CO2 sequestration experiments. In: Greenh. Gas control technol. Int. Conf.; 2003. p. 1667–70.
[317] Brewer PG, Peltzer E, Aya I, Haugan P, Bellerby R, Yamane K, Kojima R, Walz P, Nakajima Y. Small scale field study of an ocean CO2 plume. J Oceanogr 2004;60:751–8.
[318] Tsouris C, Brewer P, Peltzer E, Walz P, Riestenberg D, Liang L, West OR. Hydrate composite particles for ocean carbon sequestration: field verification. Environ Sci \& Technol 2004;38:2470–5.
[319] Rehder G, Kirby SH, Durham WB, Stern LA, Peltzer ET, Pinkston J, Brewer PG. Dissolution rates of pure methane hydrate and carbon-dioxide hydrate in undersaturated seawater at 1000-m depth. Geochim Cosmochim Acta 2004;68:285–92.
[320] Hester KC, Peltzer ET, Walz PM, Dunk RM, Sloan ED, Brewer PG. A natural hydrate dissolution experiment on complex multi-component hydrates on the sea floor. Geochim Cosmochim Acta 2009;73:6747–56.
[321] Brewer PG, Peltzer ET, Walz PM, Coward EK, Stern LA, Kirby SH, Pinkston J. Deep-sea field test of the CH4 hydrate to CO2 hydrate spontaneous conversion hypothesis. Energy \& Fuels 2014;28:7061–9.
[322] Dhamu V, Qureshi MF, Abubakar S, Usadi A, Barckholtz TA, Mhadeshwar AB, Linga P. Investigating high-pressure liquid CO2 hydrate formation, dissociation kinetics, and morphology in brine and freshwater static systems. Energy \& Fuels 2023;37:8406–20.
[323] Dhamu V, Qureshi MF, Barckholtz TA, Mhadeshwar AB, Linga P. Evaluating liquid CO2 hydrate formation kinetics, morphology, and stability in oceanic sediments on a lab scale using top injection. Chem Eng J 2023;478:147200.
[324] Qureshi MF, Khraisheh M, AlMomani F. Probing the effect of various water fractions on methane (CH4) hydrate phase equilibria and hydrate inhibition performance of amino acid L-proline. J Mol Liq 2021;333:115888.
[325] Qureshi MF, Khraisheh M, Almomani F. Doping amino acids with classical gas hydrate inhibitors to facilitate the hydrate inhibition effect at low dosages. Greenh Gases Sci Technol 2020;10:783–94.
[326] Khandelwal H, Qureshi MF, Zheng J, Venkataraman P, Barckholtz TA, Mhadeshwar AB, Linga P. Effect of l-tryptophan in promoting the kinetics of carbon dioxide hydrate formation. Energy \& Fuels 2020;35:649–58.
[327] Qureshi MF, Dhamu V, Usadi A, Barckholtz TA, Mhadeshwar AB, Linga P. CO2 hydrate formation kinetics and morphology observations using high-pressure liquid CO2 applicable to sequestration. Energy \& Fuels 2022;36:10627–41.
[328] Dhamu V, Mengqi X, Qureshi MF, Yin Z, Jana AK, Linga P. Evaluating CO2 hydrate kinetics in multi-layered sediments using experimental and machine learning approach: applicable to CO2 sequestration. Energy 2024;290:129947.
[329] Jeenmuang K, Pornaroontham P, Qureshi MF, Linga P, Rangsunvigit P. Micro kinetic analysis of the CO2 hydrate formation and dissociation with L-tryptophan in brine via high pressure in situ Raman spectroscopy for CO2 sequestration. Chem Eng J 2024;479:147691.
[330] Biniek K, De Luna P, Di Fiori L, Hamilton A, Stackhouse B. Scaling the CCUS industry to achieve net-zero emissions. McKinsey's Oil Gas Pract. 2022 https

://www.mckinsey.com/industries/oil-and-gas/our-insights/scaling-the-ccus-industry-to-achieve-net-zero-emissions.
[331] Nguyen NN, La VT, Huynh CD, V Nguyen A. Technical and economic perspectives of hydrate-based carbon dioxide capture. Appl Energy 2022;307:118237.
[332] Wang J, Ryan D, Anthony EJ, Wildgust N, Aiken T. Effects of impurities on CO2 transport, injection and storage. Energy Procedia 2011;4:3071–8.
[333] Z.E.P. Secretariat. The cost of subsurface storage of CO2. zeroemissionsplatform.eu/co2-storage-cost/, https://zeroemissionsplatform.eu/co2-storage-cost/; 2019.
[334] Sinehbaghizadeh S, Saptoro A, Mohammadi AH. CO2 hydrate properties and applications: a state of the art. Prog Energy Combust Sci 2022;93:101026.
[335] Global Status of CCS 2022 report. Global CCS Institute; 2022. https://status22.globalccsinstitute.com/2022-status-report/introduction/.
[336] United States Geological Survey, (n.d.). https://www.usgs.gov/media/images/map-gas-hydrates.
[337] Filippov SP, Yaroslavtsev AB. Hydrogen energy: development prospects and materials. Russ Chem Rev 2021;90:627.
[338] Metz B, Davidson O, De Coninck HC, Loos M, Meyer L. IPCC special report on carbon dioxide capture and storage. Cambridge: Cambridge University Press; 2005.